IJHSR

International Journal of High School Research

February 2019 | Volume 1 | Issue 1
ijhighschoolresearch.org

GENIUS Olympiad

"Lets build a better future together"

GENIUS Olympiad, the largest international environmental science high school project competition, promotes a global understanding of environmental issues and the achievement of sustainability through basic science, arts, creative writing, engineering, design, and business development. GENIUS Olympiad provides challenges and opportunities for secondary school students to instill in them the skills and knowledge needed to be the citizens, leaders, scientists, artists, writers, engineers, and policy makers of the future-agents who will promote and contribute to greater environmental sustainability throughout their lives.

Categories

Science

GENIUS Science provides understanding and solutions to environmental problems using scientific knowledge.

VPA

Short Film, Poster Design, & Photography

GENIUS Visual and Performance Arts heightens public concern for environmental problems and solutions.

Business

Entrepreneurship & Social Responsibility

GENIUS Business raises awareness of environmental values and social responsibility in the business world.

Writing

Poetry, Fiction, Essay

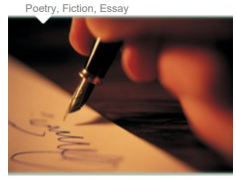

GENIUS Creative Writing raises awareness about environmental problems, calling us to action on solutions.

Robotics

Robots & Drones

GENIUS Robotics provides engineering and automation solutions to resolve given environmental issues.

GENIUS 2018 at a Glance

1,026 Students

72 Countries

35 States

1,704 Projects Submitted

274K Website Visits

"I commend all affiliated with this ambitious project for your hard work and commitment to creating a better future for our world."

Andrew Cuomo
Governor

"This event taps into SUNY's commitment to promoting sustainability and environmental awareness. I'm so proud that SUNY Oswego is hosting this global forum for the next generation to explore cross-discipline strategies to ensure humanity's survival on this planet. Raising our collective consciousness of what's happening to the environment will pave the way to a better future. It is through gatherings like this that new leaders will emerge, and fresh ideas will flourish."

Kristina M. Johnson
SUNY Chancellor

Organized & Sponsored by:

terra science and education

www.geniusolympiad.org

Hosted by:

OSWEGO STATE UNIVERSITY OF NEW YORK

INTERNATIONAL JOURNAL OF HIGH SCHOOL RESEARCH

www.ijhighschoolresearch.org

CONTENTS

FEBRUARY 2019 VOLUME 1 ISSUE 1

International Program Opportunities

The American Commission of Accreditation for Schools and Universities (ACASU) aims to endorse the highest quality education for students to lead to a lifetime of achievement and service to others in a connected world.

www.acasu.org
info@acasu.org

Genius Olympiad is the second largest international high school project competition hosted in the United States. Students compete in five disciplines to solve environmental issues and participate in a week of cultural events with 1400+ participants from 70+ countries.

www.geniusolympiad.org
info@geniusolympiad.org

International Research Collaborations is a new and unique program that features opportunities for participating students to engage in a scientific and cultural exchange between schools in different countries. The collaborations will be patterned after the long-running programs between American, South Korean, and Singapore students featured in *Nature 2015*.

www.internationalresearchcollaborations.org
rbeal@terraed.org

International SAT Prep Course

Terra offers international secondary schools a 4-week course to prepare students for the American SAT exam that is required for most American University applications.

The SAT teacher comes to your school and you choose the dates of your program

For details visit:
www.geniusolympiad.org.

About the Cover

The first issue of IJHSR features the artwork of James Christopher Talens, a student from the Philippines studying at Pan-Asia International School in Bangkok, Thailand.

Want to submit your artwork to be featured on the next cover? Send your work to editor@terraed.org.

Teach Abroad

Terra Science and Education offers a paid internship for American graduate education students and retired certified teachers to teach English abroad.

International schools interested in hosting an American teacher should contact Terra at info@terraed.org.

For details visit:
www.terraed.org

Contact Us:
835 W Genesee Street
Syracuse, NY 13204
P: +1 (315) 422-2902
E: info@terraed.org

Follow Terra Science and Education on:

Editorial Board

Introducing the International Journal of High School Research

Learn More About IJHSR:

The International Journal of High School Research aims to select the highest quality of student work to represent the future of the scientific community. Two issues will be published each year with selections of a variety of student work from around the world.

Only manuscripts prepared according to template guidelines will be considered for review. The template guideline can be downloaded on the IJHSR website at ijhighschoolresearch.org. For any questions, please send an email to editor@terraed.org.

Why Publish with IJHSR?

Students gain experience writing for a scientific journal which may help their college applications stand out. IJHSR is unique in that high school students from around the globe are published together. Students can see how they stack up to other students internationally and read the work of their peers around the world.

Student work is published at no cost to the student, the student's mentors/teachers, or the student's institution.

Want to Become an Editor?

You can request to join the editorial boad or the youth editorial board by emailing your credentials to editor@terraed.org.

After joining the IJHSR Editorial team, you will be sent student manuscripts in the categories you are qualified to review. Reviews are requested to be conducted within a week of the date they are sent.

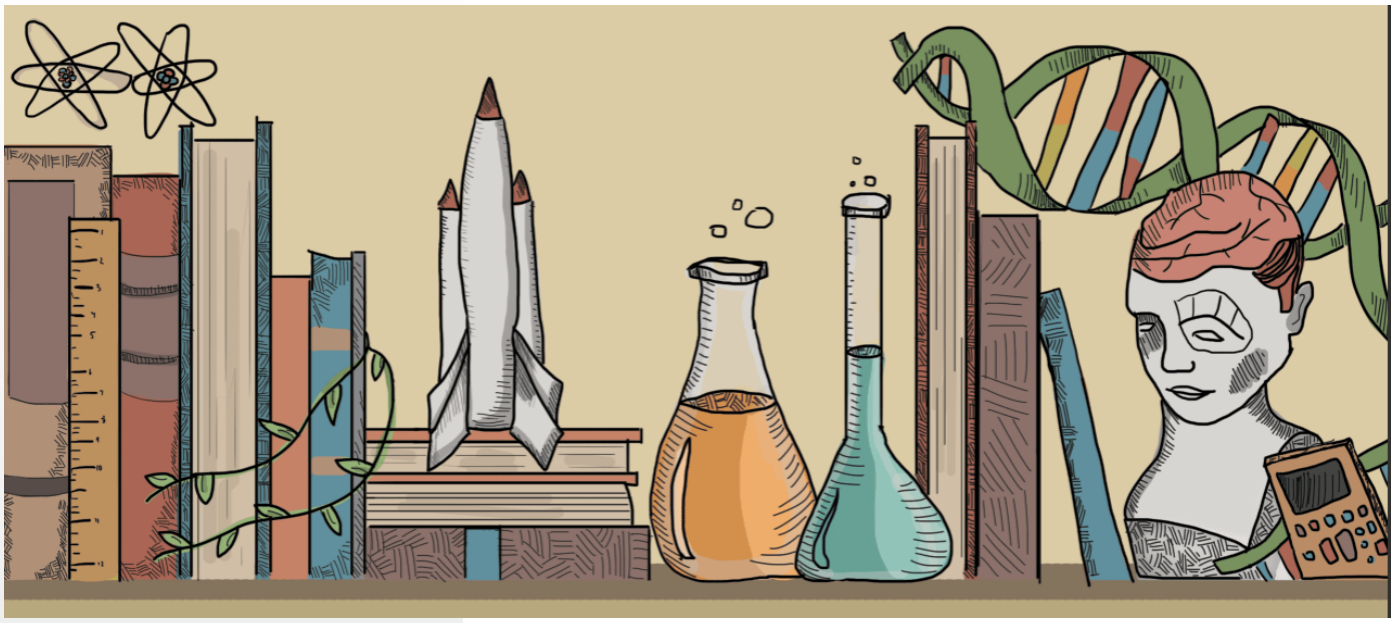

Qualifications

High school students from any country can submit their research to be considered for publication in the International Journal of High School Research. Preference is given to students who have received an award for their work. Research categories include, but are not limited to:

Agriculture
Astronomy
Biochemistry
Biology
Botany
Chemistry
Computer Science
Earth and Atmospheric
Engineering
Genetics
Geology
Mathematics
Nanotechnology
Pharmacology
Physics
Physiology
Statistics
Zoology

Submit Your Work To IJHSR

How to Apply

Please read the guidelines on the IJHSR website at ijhighschoolresearch.org before submitting your work. Download the IJHSR submission template as a Word Document to help structure your paper in the proper format.

ALL research papers should be titled as follows:
YearMonthDay_LastName_FirstName

For papers with multiple authors:
LastName(1)_LastName(2)

Send all submissions in the proper formatting to editor@terraed.org.

For further questions, please refer to the Facts and Questions page ("FAQ") on ijhighschoolreasearch.org
or
email editor@terraed.org.

“Is There Anybody Out There?” Gamma Ray Bursts and the Fermi Paradox

Susanna Weber [1], Luis Anchordoqui [2] (mentor)

1. *Mamaroneck High School, 1000 Boston Post Rd., Mamaroneck, NY, 10543, United States*
2. *Department of Physics & Astronomy, Lehman College, City University of New York, NY, 10468, United States*

susamawe@gmail.com[1]
luis.anchordoqui@gmail.com[2]

Abstract

The Fermi paradox is the discrepancy between the likelihood of alien life and the absence of evidence for such emergence. Here, we derive an upper limit on the fraction of living intelligent species that develop communication technology $\langle \xi biotec \rangle$. $\langle ... \rangle$ indicates the average over all the manners in which civilizations can arise and develop such technology. Following Drake, we factorize $\langle \xi biotec \rangle$ as the product of the fractions in which: (i) life arises, (ii) intelligence develops, and (iii) communication technology is developed. This averaging procedure is an approximation because the characteristics of the initial conditions in a planet and its surroundings affect the phenomena with high complexity. The number of communicating t civilizations that exist in the galaxy is formulated to be $N = \langle \zeta astro \rangle \langle \xi biotec \rangle L_T$. $\langle \zeta astro \rangle$ is the average production rate of habitable planets; L_τ is the length of time that a civilization communicates. Using determinations of the characteristics of gamma-ray bursts (GRBs), we calculate the probability that a GRB could make a planet inhospitable, yielding $\langle \zeta astro \rangle \sim 2 \times 10^{-3}$. Our current measurement of N = 0 implies $\langle \zeta biotec \rangle < 5 \times 10^{-3}$ at the 95% confidence level, where we have taken $L_\tau > 0.3$ Myr such that $L\tau >>>$ propagation distances of Galactic scales (~10 kpc).

Keywords

Astrophysics; High Energy Astrophysics; Gamma Ray Bursts; Extraterrestrial Life; Fermi Paradox; Drake Equation

Introduction

On May 25,1961, President Kennedy's announcement to put a man on the moon and bring him back safely before the end of the decade initiated the advent of human exploration of space for NASA, culminating in the landing on the Moon on July 16, 1969. Considering the immense size and age of the universe, it is difficult to believe that this event is unique. On the other hand, if there is alien life capable of pulling off such a feat we must ask, as Fermi did, where is everybody?[1] In a first approximation of the answer, we can model the number of intelligent civilizations in our galaxy at any given time capable of releasing detectable signals of their existence into space using a quite simple functional form,

$$N = R_* f_p n_e f_\ell f_i f_c L_\tau \quad (1)$$

where R_* is the average rate of star formation, f_p is the fraction of stars with planetary systems, n_e is the number of planets (per solar system) with a long-lasting (~4 Gyr) ecoshell, f_ℓ is the fraction of suitable planets on which life actually appears, f_i is the fraction of living species that develop intelligence, f_c is the fraction of intelligent species with communications technology, and L_τ is the length of time such civilizations release detectable signals into space (i.e. the lifetime of the communicative phase).[2] Following Prantzos,[3] we separate (1) into its astrophysical and biotechnological factors:

$$N = \langle \zeta astro \rangle \langle \xi biotec \rangle L_\tau \quad (2)$$

Where $\langle \zeta astro \rangle = R_* f_p n_e$ represents the production rate of habitable planets with long-lasting ecoshells (determined through astrophysics) and $\langle \xi biotec \rangle = f_l f_i f_c$ represents the product of all chemical, biological and technological factors leading to the development of a technological civilization. $\langle \cdots \rangle$ indicates the average over all the multiple means in which civilizations can arise, grow, and develop such technology, starting at any time since the formation of our galaxy in any location inside it. This averaging procedure must be regarded as a crude approximation because the characteristics of the initial conditions on a planet and its surroundings may affect $f_\ell f_i f_c f_c$ with high complexity. In this work we estimate the production rate of exoplanets in the habitable zone and the rate of planetary catastrophes which could threaten the evolution of life on the surface of these worlds. Armed with these estimates, we use our current measurement of N = 0 to set an upper limit on $\langle \xi biotec \rangle$ N = 0 is referring to the case of "another" sufficiently advanced race we could detect.

Results and Discussion

The Drake Equation

The star formation rate in the galaxy is estimated to be $M_* = 1.65 \pm 0.19 M_\odot tyr^{-1}$.[4,5] This estimate has been derived assuming the Kroupa initial mass function (IMF).[6,7] The shape of this IMF is lognormal-like and exhibits a peak around $M / M_\odot \approx 0.4$,[8] suggesting there are roughly 2 stars per M. Altogether, this yields $R_* \approx 3 yr^{-1}$. Now, only 10% of these stars are appropriate for harboring habitable planets. This is because the mass of a star $M_\otimes$ must be $< 1.1 M_\odot$ to be sufficiently long-lived (with main sequence lifetimes larger than 4.5 Gyr) and the mass of $M_\otimes$ must be $> 0.7 M_\odot$ to possess circumstellar habitable zones outside the tidally locked region.[9] The frequency η⊕ of terrestrial planets in the habitable zone of solar-type stars can be determined using data from the Kepler mission.[10-12] Current estimates suggest 0.15(+0.13, −0.06) < η⊕ < 0.61 (+0.07 , −0.15).[13,14] The production rate of habitable planets is then $3 yr^{-1} \times 0.1 \times 0.15 \sim 0.045 yr^{-1}$.

Gamma Ray Bursts

Next, in line with our stated plan, we estimate a rough probability that a habitable planet will survive and remain in a habitable zone to present day. Gamma-ray bursts (GRBs) are short-lived, luminous explosions, thought to originate from relativistic plasma launched at the time of deaths of massive stars. The widely accepted interpretation of GRB phenomenology is that the observable effects are due to the dissipation of the kinetic energy of a relativistically expanding fireball.[15] The physical conditions in the dissipation region produce a heavy flux of photons with energies above an estimated 100 keV. It has been suggested that a nearby (galactic) GRB may destroy the ozone layer, possibly making the GRB damaging to life on Earth. Because of this, GRBs have been proposed to explain events of massive terrestrial life extinction.[16-22] GRBs are generally divided into two groups according to their duration: long (> 2 s) and short (< 2 s). Short GRBs are weaker and hence, even though their rate is higher than the rate of long GRBs, their life-threatening effect is negligible.[22] Throughout we consider only long GRBs. We want to estimate the expected number of GRBs that can terminate life on a planet that is situated at a Galactic radius *R*. To this end we should take into account the following considerations:

The Luminosity-Rate Function

The luminosity-rate function φ(L), which measures the number of GRBs with a luminosity in a small range around a given value L occurring per unit time and volume, is given by:

$$\phi(L) = n\begin{cases}\left(\frac{L}{L^*}\right)^{-\alpha} & L_{\min} < L < L^* \\ \left(\frac{L}{L^*}\right)^{-\beta} & L^* < L < L_{\max}\end{cases} \tag{3}$$

where $\alpha = 1.2(+0.2,-0.1), \beta = 2.4(+0.3,-0.6), L^* = 1052.5 \pm 0.2 ergs^{-1}, L_{\min} = 1049 ergs^{-1}, and\ L_{\max} = 1054 ergs^{-1}$.[23] Here, n is the volumetric rate of GRBs at $L = L^*$. We consider a fiducial value of $n_0 = 0.15(+0.7,-0.8) yr^{-1} Gpc^{-3}$.[23] To accommodate the metallicity bias determined in Jimenez et al.,[24] we follow Piran et al. and take correction of a factor 10.[22] It has been noted in Gowanlock that such a low metallicity correction factor yields an upper limit on the volumetric rate of long GRBs $n \leq 0.1 n_0$.[25] To derive our upper bound on $\langle \xi biotec \rangle$ we will adopt $n = 0.1 n_0$, since the larger the number of GRBs, the smaller the number of planets with a long-lasting ecoshell, and therefore the larger the value of $\langle \xi biotec \rangle$ In general, any GRB regardless of its luminosity could terminate life if it is close enough to a planet. This is taken into account in our next point.

The Fluence

The fluence $\mathfrak{F}$ measures the amount of energy per unit area arriving to a planet from a distant GRB. If the distance between the GRB and the planet is r, an isotropic emission and conservation of energy implies

$$\mathfrak{F} = \frac{E}{4\pi r^2} \tag{4}$$

where E is the total energy released by the GRB. The effects of a copious flux of gamma rays on the Earth's atmosphere have been studied in Thomas et al.[19,20] A fluence of $10 \mathrm{kJ}/m^2$ could cause a depletion of roughly 68% of the ozone layer on a time scale of a month, whereas fluences of $100 \mathrm{kJ}/m^2$ and $1000 \mathrm{kJ}/m^2$ could cause depletions of about 91% and 98%, respectively. This implies that a fluence of $10 \mathrm{kJ}/m^2$ could cause some damage to life, while $1000 \mathrm{kJ}/m^2$ will wipe out nearly the whole atmosphere causing a catastrophic life extinction event. Note, however, that the complete removal of all life on an Earth-like planet is a very unlikely event.[26] The critical fluence $\mathfrak{F}_c$ gives the limit on acceptable fluence on a planet. In our calculations we take $\mathfrak{F}_c^* = 100 kJ/m^2$ as our fiducial life threatening critical fluence.[22]

The Hazard Distance

The hazard distance of a GRB, characterized by its total energy *E*, measures the length for which the fluence is higher than the critical fluence $\mathfrak{F}_c$. Any planet within this distance will have life terminated. For a fixed GRB energy and critical fluence, we use (4) to obtain the hazard distance:

$$d(L, F_c) = \sqrt{\frac{E}{4\pi F_c}} = \sqrt{\frac{L_\tau}{8\pi F_c}} \tag{5}$$

where in the second rendition we have assumed that the total GRB energy is roughly the average (~ half) of the peak flux $E = L_\tau / 2$.[22] A good but rough estimate of E follows from the assumption that the typical duration of long GRBs is τ ~20 s.[15]

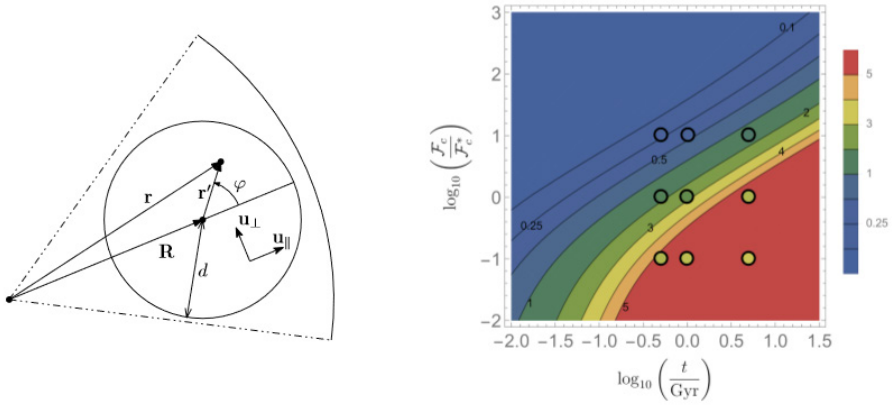

Figure 1: Hazard region (left) and probability contours for life destroying GRB on Earth as function of total time t and critical fluency $\mathfrak{F}_c$ normalized to $\mathfrak{F}_c^* = 100kJ/m^2$ (right). We have taken $R_{(solar\ system)} \approx 8.12\text{kpc}$.

The Fraction of Hazardous Galaxy

The fraction of hazardous galaxy $p[d,R]$ measures the fraction of the total galactic mass that is within the hazard distance *d*, for any point at radius *R* from the galactic center. The fraction of galactic mass that is contained within a surface element at radius *r* is given by,

$$\rho(r) = \frac{1}{2\pi r_d^2} e^{\left(-\frac{r}{r_d}\right)} \tag{6}$$

such that $\int \rho(r)\mathbf{d}a = 1$. Here, $r_d = 2.15 \pm 0.14\text{kpc}$.[26] As illustrated in Fig.1 to calculate the fraction of hazardous galaxy around a point with radius R, one has to integrate (6) in a circular region of radius d centered at $\mathbf{R}$,

$$\rho[d,R] = \frac{1}{2\pi r_d^2} \int_s e^{-\frac{r}{r_d}} \mathbf{d}a \tag{7}$$

Defining the unit vectors $\mathbf{u}_{\|} = \mathbf{R}/R$ and $\mathbf{u}_{\perp}$ perpendicular to $\mathbf{u}_{\|}$ we can write $\mathbf{R} = R\mathbf{u}_{\|}$ and $\mathbf{r}' = r'(\cos\varphi \mathbf{u}_{\|} + \sin\varphi \mathbf{u}_{\perp})$. Since $\mathbf{r} = \mathbf{R} + \mathbf{r}$,

$$r = |\mathbf{r}| = \sqrt{R^2 + r'^2 + 2r'R\cos\varphi} \tag{8}$$

Defining $r' \equiv zd$ we have $\mathbf{d}a = d^2 \mathbf{z}\mathbf{d}\mathbf{z}\mathbf{d}\varphi$ where z runs from 0 to 1, so that

$$p[d,R] = \frac{d^2}{2\pi r_d^2} \int_0^{2\pi} d\varphi \int_0^1 \mathbf{d}z z \ \exp\left(-\frac{1}{r_d}\sqrt{R^2 + d^2 z^2 + 2dRz\cos\varphi}\right) \tag{9}$$

The Rate of Life-Threatening Gamma Ray Bursts

The rate of life-threatening GRBs at any position of the galaxy, specified by the radius R, is given by

$$\Gamma(R,F_c) = \frac{V(M_*)}{L^*} \int_{L_{\min}}^{L_{\max}} \phi(L) p[d(L,F_c),R]\mathbf{d}L \tag{10}$$

The cosmological volume of a galaxy, with stellar mass M_*, is defined by $V(M_*) = M_*/\rho_*(z)$ where $\rho_*(z) = 10^{17.46-0.39z} M_\odot Gpc^{-3}$ is the average stellar density as a function of redshift z.[28] For a galaxy like our own Milky Way, $M_* \approx 6*10^{10} M_\odot$ and so at $z = 0$ we have $V(M_*) \sim 10^{-7} Gpc^3$.[29]

Taking into account all of these considerations, we now turn to estimating the expected number of GRBs that can terminate life in a planet situated at a galactic radius R. As it turns out $\Gamma(R,\mathfrak{F}_c)$ is $\mathcal{O}\left(Gyr^{-1}\right)$. This means that for Gyr time scales, we expect to have (on average) a small number of GRB events. This kind of estimate is then well suited to Poisson statistics. The Poisson distribution is a discrete probability distribution for the counts of events that occur randomly in a given interval of time (or space). Of particular interest here, the probability of having ***i*** GRBs when the expected average μ, is given by $p_i = e^{-\mu}\mu^i / \mathbf{i}$. The probability of having 1 or more GRBs is

$p = \sum_{i=1}^{\infty} p_i = 1 - p_0 = 1 - e^{-\mu}$. The average number of GRBs during a time t is ì =Γ(R,ℑ$_c$)t t, and therefore

$$p\left(t, R\mathfrak{F}_c\right) = 1 - e\,\wedge\left(-\Gamma^{(R,\mathfrak{F}_c)t}\right) \tag{11}$$

In Fig. 1 we show probability contours of at least one GRB having occurred in the past time t with enough flux to produce significant life extinction on Earth. Since the probabilities get too high in most of the parameter space of interest, the legend does not show the probability p (which would be too close to 1), but instead the parameter k defined by

$$p = \frac{1}{\sqrt{(2\pi)}} \int_{-k}^{+k} e^{-x^2/2} \mathbf{d}x \tag{12}$$

Since $\mathbf{r} = \mathbf{R} + \mathbf{r}$,

which gives the usual correspondence between probabilities and the standard deviation for a normal distribution, which leads to $k = \sqrt{2} Erf^{-1}(p)$. Some value correspondences between k and the probabilities in % are $k = 1 \leftrightharpoons 68\%, k = 2 \leftrightharpoons 95.5\%,$ and $k = 5 \leftrightharpoons 99.99994\%$. The circles indicate selected values of $\mathfrak{F}_c / (kJ/m^2) = 10, 100, 1000$ and t$/\,Gyr = 0.5, 1, 5$. Our estimates are in good agreement with those given in Table II of Piran et al.[22] These findings seem to indicate that a nearby GRB may have caused one of the five greatest mass extinctions on Earth. However, it is important to remind the reader that the estimates shown in Fig.1 rely on an upper limit of the volumetric rate of long GRBs; namely,

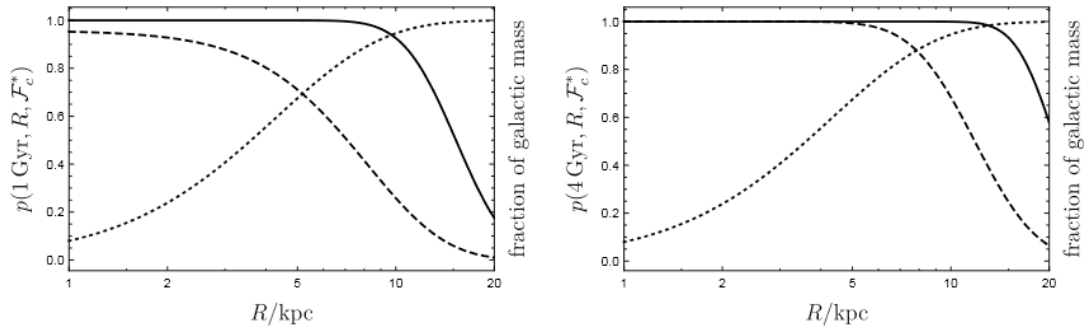

Figure 2: The probability of having one or more lethal GRBs in 1 Gyr (left) and 4 Gyr (right) for a critical fluency $\mathfrak{F}_c = 100 kJ/m^2$, as a function of distance from the galactic center. The solid line corresponds to $n = n_0$ and the long-dashed line to $n = 0.1 n_0$. Following the right legend, the short-dashed line measures the total amount of mass enclosed in a radius less than R.

Coming back to our calculation, we can use (11) to compute the probability of having at least one lethal GRB, for a critical fluency $\mathfrak{F}_c$ and a fixed lookback time t_c, as a function of the distance R. Life has been evolving on Earth for close to 4 Gyr,[30,31] but complex life is well under 1 Gyr old, and intelligent life is only one Myr old at most. In what follows, we adopt $t_c = 1$ Gyr and 4 Gyr as critical time intervals for life evolution.[32] In Fig. 2 we show the probability of having one or more lethal GRBs for a critical fluency $\mathfrak{F}_c = 100 kJ/m^2$ and $t_c / Gyr = 1$ and 4, as a function of distance from the galactic center.

All we need to do now is add the components together to arrive at the production rate of habitable planets with a long-lasting ecoshell,

$$\langle \zeta astro \rangle = 0.045 yr^{-1} \int_0^{\infty} \int_0^{2\pi} \left[1 - p\left(t, R, \mathfrak{F}_c\right)\right] \boldsymbol{\rho}\left(R\right) \mathbf{d}\varphi R \mathbf{d}R \tag{13}$$

It is of interest to study how $\langle \zeta astro \rangle$ depends on the different parameters involved. According to (3), (10) and (11), the dependence of p in n and t can be grouped in the same functional dependence. Introducing $\Gamma_0 \equiv \Gamma|_{n=n_0}$ one can rewrite $\Gamma_t = x \Gamma_0 t_0$ where $x = (t/t_0)(n/n_0)$ and $t_0 = Gyr$. We can then rewrite (13) $\langle \zeta astro \rangle = 0.045 yr^{-1} \mathfrak{J}(x)$ where

$$\mathfrak{J}\left(x\right) = 2\pi \int_0^{\infty} \exp\left[-x\right] \Gamma_0\left(R, \mathfrak{F}_c\right) t_0 \boldsymbol{\rho}(R) R \mathbf{d}R \tag{14}$$

The value of $\mathfrak{J}(x)$ is shown in Fig. 3 as a function of $x < 0.4$ for different values of $\mathfrak{F}_c$. Note that for $\mathfrak{F}_c = 100 \mathrm{kJ/m^2}$, with $t_c = Gyr$ and $4 Gyr$, (13) leads to $\langle \zeta astro \rangle = 1 x 10^{-2}$ and 2×10^{-3}, respectively.

Finally, to determine the upper bound on $\langle \xi biotec \rangle$ we must decide on the possible minimum L_τ. Herein we consider $L_\tau > 0.3$ Myr such that $cL_\tau \ggg$ propagation distances of Galactic scales (~10 kpc, or 100,000 light years). This would provide enough time to receive electromagnetic (and/or high-energy neutrino)[33] signals from any advanced civilization living in the Milky Way which is trying to communicate with us, or another civilization.

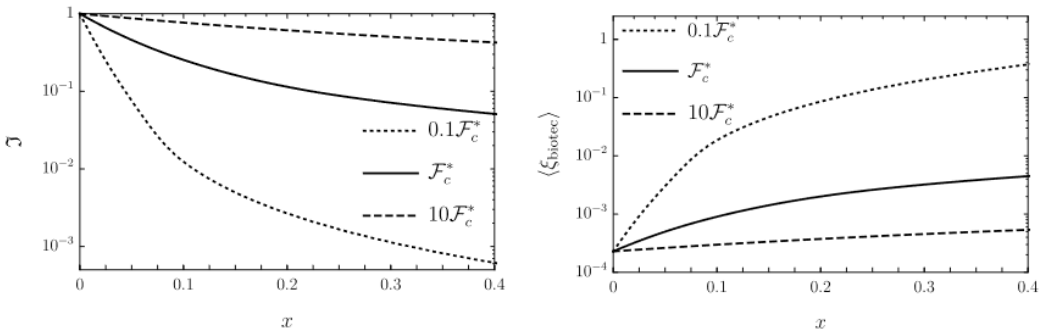

Figure 3: The integral $\mathfrak{F}$ (left) and the variation of the upper limit on $\langle \xi biotec \rangle$ (right) as a function of x, for three different hazardous fluences.

As of today, the non-observation of evidence of advanced civilizations implies that models of $\langle \xi biotec \rangle$ predicting N > 3.09 are excluded at the 95% C.L.[34] Assuming that evolution requires 4 Gyr for life to evolve and that the communication phase with advanced civilizations must last at least 0.3 Myr, we obtain $\langle \xi biotec \rangle < 5x10^{-3}$ at the 95% C.L. If instead we consider that only 1Gyr would be required (on average) or intelligent life to evolve the 95% C.L. upper limit becomes more restrictive: $\langle \xi biotec \rangle < 1x10^{-3}$. The dependence of $\langle \xi biotec \rangle$ on x is shown in Fig. 3. A closing argument is that our estimate for the production rate of habitable planets is overly conservative, as we have adopted the present-day star formation rate. It has been noted that the average star formation rate in the galaxy could be about 4 times the current rate.[35]

Conclusion

In summary, in this paper we have derived an upper bound on the average fraction of living intelligent species that develop communication technology: $\langle \xi biotec \rangle < 5x10^{-3}$ at the 95% C.L. Future observations could help to tighten this bound. In particular, a new arsenal of data will certainly provide an ideal testing ground to improve our understanding about: (i) the occurrence of exoplanets in the habitable zone, (ii) the early star formation rate models, and (iii) the GRB phenomenology. Though there are factors that affect the development and sustainability of life that are impossible to measure, such as geological or cultural effects, this research represents an important starting point in using empirical models to answer questions about the possibility of life in the galaxy. The past few years have witnessed the discovery of more and more rocky planets that are larger and heftier than Earth. Finding the Earth-twins is a higher order challenge, because these smaller planets produce fainter signals. Technology to detect and image Earth-like planets has been developed for use of the next generation space telescopes. The Transiting Exoplanet Survey Satellite (TESS)[36] is NASA's next step in the search for planets outside of our solar system, including those that could support life. The NASA roadmap will subsequently continue with the launch of the James Webb Space Telescope (JWST)[37] and perhaps the proposed Wide Field Infrared Survey Telescope - Astrophysics Focused Telescope Assets (WFIRST-AFTA) early in the next decade.[38] The ability to detect alien life may still be many years away, but the quest is underway.

Acknowledgements

We thank Michael Unger for discussion and Pink Floyd for inspiration. Special thanks to Mr. Garbarino at Mamaroneck High School for his assistance. This research was supported by the U.S. NSF (Grant PHY-1620661) and NASA (Grant NNX13AH52G).

References

1. E. M. Jones, Where is everybody?, An account of Fermi's Question, LA-10311-MS, UC-34b, CIC-14 Report Collection, March 1985; Physics Today38, p.11 August 1985, (without full correspondence). http://www.fas.org/sgp/othergov/doe/lanl/la-10311-ms.pdf
2. F. D. Drake, The radio search for intelligent extraterrestrial life, in Current aspects of exobiology, (Eds. G. Mamikunian and M. H. Briggs, Elsevier Ltd., 1965), p.323. ISBN: 978-1-4832-0047-7
3. N. Prantzos, A joint analysis of the Drake equation and the Fermi paradox, Int. J. Astrobiol.12, 246 (2013) doi:10.1017/S1473550413000037 [arXiv:1301.6411].
4. T. C. Licquia and J. A. Newman, Improved estimates of the Milky Way's stellar mass and star formation rate from hierarchical bayesian meta-analysis, Astrophys. J.806, 96 (2015) doi:10.1088/0004-637X/806/1/96 [arXiv:1407.1078].
5. L. Chomiuk and M. S. Povich, Toward a unification of star formation rate determinations in the Milky Way and other galaxies, Astron. J.142, 197 (2011) doi:10.1088/0004-6256/142/6/197 [arXiv:1110.4105].
6. P. Kroupa, The initial mass function of stars: Evidence for uniformity in variable systems, Science 295, 82 (2002) doi:10.1126/science.1067524 [astro-ph/0201098].
7. P. Kroupa and C. Weidner, Galactic - field IMFs of massive stars, Astrophys. J.598, 1076 (2003) doi:10.1086/379105 [astro-ph/0308356].
8. C. J. Lada, Star formation in the local Milky Way, arXiv:1508.02711.
9. S. Seager, Exoplanet habitability, Science,340, 577 (2013) doi: 10.1126/science.1232226
10. W. J. Borucki et al. [Kepler Collaboration], Kepler planet-detection mission: Introduction and first results, Science327, 977 (2010). doi:10.1126/science.1185402
11. W. J. Borucki et al. [Kepler Collaboration], Characteristics of planetary candidates observed by Kepler, II: Analysis of the first four months of data, Astrophys. J.736, 19 (2011) doi:10.1088/0004-637X/736/1/19 [arXiv:1102.0541].
12. N. M. Batalha et al. [Kepler Collaboration], Planetary candidates observed by Kepler, III: Analysis of the first 16 months of data, Astrophys. J. Supp.204, 24 (2013) doi:10.1088/0067-0049/204/2/24 [arXiv:1202.5852].
13. C. D. Dressing and D. Charbonneau, The occurrence rate of small planets around small stars, Astrophys. J.767, 95 (2013) doi:10.1088/0004-637X/767/1/95 [arXiv:1302.1647].
14. R. k. Kopparapu, A revised estimate of the occurrence rate of terrestrial planets in the habitable zones around Kepler M-dwarfs, Astrophys. J.767, L8 (2013) doi:10.1088/2041-8205/767/1/L8 [arXiv:1303.2649].
15. T. Piran, Gamma-ray bursts and the fireball model, Phys. Rept.314, 575 (1999) doi:10.1016/S0370-1573(98)00127-6 [astro-ph/9810256].
16. M. A. Ruderman, Possible consequences of nearby supernova explosions for atmospheric ozone and terrestrial life, Science185, 1079 (1974).
17. S. E. Thorsett, Terrestrial implications of cosmological gamma-ray burst models, Astrophys. J.444, L53 (1995) doi:10.1086/187858 [astro-ph/9501019].
18. A. Dar, A. Laor and N. J. Shaviv, Life extinctions by cosmic ray jets, Phys. Rev. Lett.80, 5813 (1998) doi:10.1103/PhysRevLett.80.5813 [astro-ph/9705008].
19. B. C. Thomas, C. H. Jackman, A. L. Melott, C. M. Laird, R. S. Stolarski, N. Gehrels, J. K. Cannizzo and D. P. Hogan, Terrestrial ozone depletion due to a Milky Way gamma-ray burst, Astrophys. J.622, L153 (2005) doi:10.1086/429799 [astro-ph/0411284].
20. B.C.Thomas et al.,Gamma-ray bursts and the Earth: Exploration of atmospheric, biological, climatic and biogeochemical effects, Astrophys. J.634, 509 (2005) doi:10.1086/496914 [astro-ph/0505472].
21. A. Melott et al., Did a gamma-ray burst initiate the late Ordovician mass extinction?, Int. J. Astrobiol. 3, 55 (2004) doi:10.1017/S1473550404001910 [astro-ph/0309415].
22. T. Piran and R. Jimenez, Possible role of gamma-ray bursts on life extinction in the Universe, Phys. Rev. Lett.113, 231102 (2014) doi:10.1103/PhysRevLett.113.231102 [arXiv:1409.2506].
23. D. Wanderman and T. Piran, The luminosity function and the rate of Swift's gamma-ray bursts, Mon. Not. Roy. Astron. Soc.406, 1944 (2010) doi:10.1111/j.1365-2966.2010.16787.x [arXiv:0912.0709].
24. R. Jimenez and T. Piran, Reconciling the gamma-ray burst rate and star formation histories, Astrophys. J.773, 126 (2013) doi:10.1088/0004-637X/773/2/126 [arXiv:1303.4809].
25. M. G. Gowanlock, Astrobiological effects of gamma-ray bursts in the Milky Way galaxy, Astrophys. J.832, 38 (2016) doi:10.3847/0004-637X/832/1/38 [arXiv:1609.09355].
26. D. Sloan, R. Alves Batista, and A. Loeb, The resilience of life to astrophysical events, Scientific Reports (to be published).
27. J. Bovy and H. W. Rix, A direct dynamical measurement of the Milky Way's disk surface density profile, disk scale length, and dark matter profile at 4 kpc < ∼R < ∼9 kpc, Astrophys. J.779, 115 (2013) doi:10.1088/0004-637X/779/2/115 [arXiv:1309.0809].

28. Y. Li and B. Zhang, Can life survive gamma-ray bursts in the high-redshift universe?, Astrophys. J. 810, 41 (2015) doi:10.1088/0004-637X/810/1/41 [arXiv:1507.05966 [astro-ph.HE]].
29. P. J. McMillan, Mass models of the Milky Way, Mon. Not. Roy. Astron. Soc.414, 2446 (2011) doi:10.1111/j.1365-2966.2011.18564.x [arXiv:1102.4340 [astro-ph.GA]].
30. S. J. Mojzsis, G. Arrhenius, K. D. McKeegan, T. M. Harrison, A. P. Nutman, and C. R. L. Friend, Evidence for life on Earth before 3,800 million years ago, Nature384, 55 (1996) doi:10.1038/384055a0.
31. M. S. Dodd, D. Papineau, T. Grenne, J. F. Slack, M. Rittner, F. Pirajno, J. O'Neil, and C. T. S. Little, Evidence for early life in Earth's oldest hydrothermal vent precipitates, Nature543, 60 (2017) doi:10.1038/nature21377.
32. A. Loeb, R. A. Batista and D. Sloan, Relative likelihood for life as a function of cosmic time, JCAP 1608, 040 (2016) doi:10.1088/1475-7516/2016/08/040 [arXiv:1606.08448 [astro-ph.CO]].
33. J. G. Learned, S. Pakvasa and A. Zee, Galactic neutrino communication, Phys. Lett. B671, 15 (2009) doi:10.1016/j.physletb.2008.11.057 [arXiv:0805.2429].
34. G. J. Feldman and R. D. Cousins, A Unified approach to the classical statistical analysis of small signals, Phys. Rev. D57, 3873 (1998) doi:10.1103/PhysRevD.57.3873 [physics/9711021].
35. R. C. Kennicutt, Jr. and N. J. Evans II, Star formation in the Milky Way and nearby galaxies, Ann. Rev. Astron. Astrophys.50, 531 (2012) doi:10.1146/annurev-astro-081811-125610 [arXiv:1204.3552].
36. https://tess.gsfc.nasa.gov
37. https://www.jwst.nasa.gov
38. https://wfirst.gsfc.nasa.gov

Authors

Susanna Weber is a Senior at Mamaroneck High School who has been doing student research in the field of Astrophysics since Sophomore year, and fascinated by space for as long as she can remember. She plans on majoring in Physics in college, and pursuing a career in research.

Boundary-Layer Flow Dynamics Concerning Forward Swept Wings

Arjay R. Mirchandani

Yorktown High School, 2727 Crompond Road, Yorktown Heights, NY 10598, United States

arjay.mirchandani@yorktown.org

Abstract

Air travel has two major issues; plane crashes caused by loss of control and its contribution to pollution. Aircrafts could employ a new wing orientation, forward swept wings, which would increase the effectiveness of the rear wing set, thereby increasing the control given to the pilot. Other studies suggest that forward swept wings are more efficient than the contemporary rear swept wings. If aircrafts became more efficient, then they could fly the same distance without consuming as much fuel, thereby decreasing air pollution emissions. This experiment measured the efficiency ratio (lift-to-drag ratio) as a proxy for fuel efficiency. I utilized force sensors to measure lift (upward force) and drag (frictional force) on 3D printed wing models in order to create the efficiency ratio (lift/drag). This ratio, in turn, allows for comparisons of efficiency concerning differing sweep orientations. It was found that forward swept wings were more efficient than rear swept wings at subsonic speeds. This warrants future research concerning the fuel efficiency of forward swept wings at varying speeds and angles of attack in direct comparison with rear swept wings.

Keywords

Forward Swept Wings; Swept Wings; Efficiency Ratio; Lift/Drag; Wind Tunnel

Introduction

General Problem

In 2013, over 8 million people were flying daily and while air travel is a widely utilized mode of transport, it has its fair share of problems.[1]

Two of the major issues with planes are the negative impacts on the environment as well as loss of control (usually stemming from pilot error). It has been estimated that aviation in developed countries, such as the United Kingdom, generates approximately 13%-15% of greenhouse gas emissions.[2]

Additionally, plane crashes due to loss of control is another issue and preliminary estimates suggest that private planes caused 22 deaths per two million travel hours. This fatality rate is substantially higher than the automobile fatality rate; one death per two million travel hours.[3] The loss of control that occurs in airplanes has a few technological nullifiers, such as winglets and a saw-tooth, which inhibit destabilizing airflow. (Table 1)

Fatality Rate for Differing Types of Aviation

Type of Flight	Fatalities per million flight hours
Airliner (Scheduled and nonscheduled Part 121)	4.03
Commuter Airline (Scheduled Part 135)	10.74
Commuter Plane (Nonscheduled Part 135 - Air taxi on demand)	12.24
General Aviation (Private Part 91)	22.43

Planecrashinfo.com

Table 1: Fatalities for different types of air travel. The "Part #" is the classification of different types of aircraft and thus have different flight codes and regulations.

Current Nullifiers for Loss of Control

Devices like the winglet are incorporated into aircrafts in order to counter loss of control. However, these devices have only a limited effect, and cannot completely alleviate the issue because pilot error is the biggest factor in airplane crashes.[4] A possible solution to this would be to implement forward swept wings which are a new type of wing that addresses the loss of control through a different path of airflow (Figures 1 & 2).

Winglets

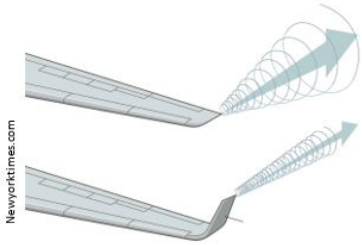

Figure 1: Diagram of winglets in action. The winglet decreases vortex generation and destabilizing airflow.

Sweep Orientations

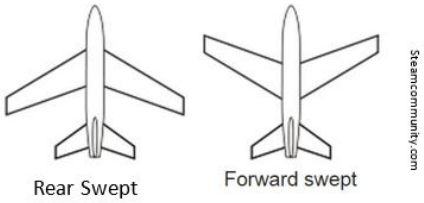

Figure 2: Comparison between rear swept and forward swept wing orientations.

The Impact on the Environment

Air travel not only emits harmful greenhouse gasses, which accelerate global warming, but the chemistry of jet emissions produces an additional warming effect. This is due to the high carbon content that is used within jet fuel, unlike many modern fuels used in other forms of travel.[5] Jet fuel, like Jet-A, has about 12 carbon atoms per molecule, while petroleum, a common base for various fuels, has about five carbon atoms per molecule.[5a, 5b] Global warming is responsible for changes in climate worldwide, leading to the need for radical changes in waste emissions[6]. The issue of carbon emissions could potentially be reduced by the implementation of forward swept wings.[15] Due to the likely improvements of efficiency, forward swept wings allow for more efficient air travel.[15, 16] This means there would be a decrease in the fuel consumption necessary for each flight, therefore reducing the amount of carbon emissions each flight produces (Figures 3 & 4). While this increase in efficiency may lead to higher demand for flights, thereby negating this improvement in efficiency (Jevons Paradox), this outcome would still result in more efficient flight from aircrafts. Furthermore, the probability of this outcome is unlikely, due to the history of similar scenarios results.[17]

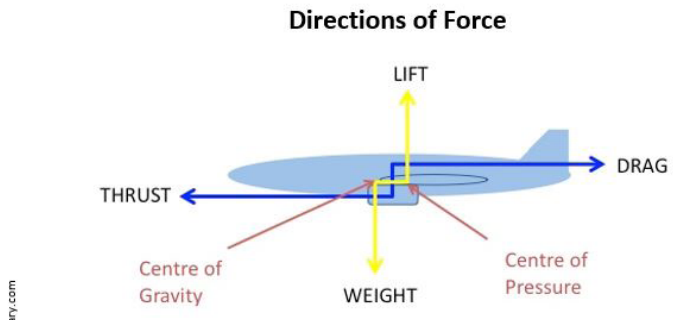

Figure 3: The direction in which a force is measured. Lift/drag defines efficiency.

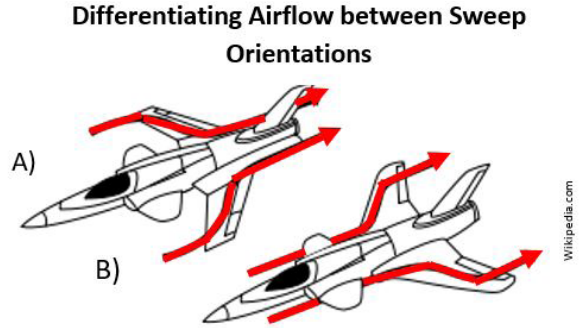

Figure 4: The airflow changes between forward swept (A) and rear swept (B) wing types.

Review of Literature

Current Aircraft Type

The most common type of airplane wing is the rear swept wing because of the high efficiency that they provide.[7] Efficiency, as defined in this experiment, is measured as the lift (upward force) divided by drag (frictional force). However, rear swept wings, while efficient, have relatively unstable airflow which makes planes much more likely to crash due to the loss of control. This instability is not fully corrected through the implementation of stabilizing components, such as winglets. The cause of the instability of rear swept wings, have been elucidated in multiple studies.[8-10]

Forward Swept Wings

The forward swept wing is a relatively unexplored option that combines high performance with reliable flight.[16] This sweep orientation was first manifested at the dawn of modern aircraft during WWII. However, this orientation was not used due to the high pressure that was put onto the wings. This pressure, after just a few flights, would critically damage the wings of the aircraft, making it unable to fly. Within the past 20 years, the prospect of using forward swept wings in contemporary aircraft design has become a viable option,[13] as the problem of high pressure was alleviated by using a modern composite material that uses fibrous layers, coupled with layered aluminum, to add to wing strength.[16] Forward swept wings lead air onto the rear wing set, causing for more stability and efficiency.[11, 12] Corrective components, such as winglets, are not required to maintain flight stability in an aircraft that uses forward swept wings due to the increased airflow displaced onto the rear wing set. Forward swept wings are predicted to be as, if not more, efficient than rear swept wings,[15, 16] which means that the forward swept orientation could generate more lift and less drag when compared to rear swept wings. With more lift and less drag being generated, the amount of fuel consumed would be lowered for flights utilizing the forward swept orientation, thereby resulting in less carbon emissions. However, even with more than ten studies focusing of the forward swept orientation, only one focused on the efficiency of the forward swept orientation due to the previously noted problem of increased pressure on the wings. No studies thus far, focused on the efficiency of forward swept wings in direct comparison to rear swept wings.

Problem

It is unknown how efficient forward swept wings are in comparison to rear swept wings. One study used a prototype of a forward swept craft, and through the process of analyzing the data from that flight, hypothesized that forward swept wings could be more efficient than rear swept wings due to the extraordinarily effective flight results gathered by the prototype's flight.[16] This study, while finding efficiency data on forward swept wings, still leaves a gap in knowledge concerning the efficiency of forward swept wings in direct comparison to rear swept wings.

Goal

The goal of this study is to test and gather preliminary efficiency values for both forward and rear swept wings, directly comparing the values. This will be done by testing and gathering data for both forward and rear swept wing types through calculating the lift and drag forces simulated via a wind tunnel in order to conclude which orientation of wing sweep is more efficient. The impact of these findings may validate the efficiency of such wings and increase its use in modern aircraft designs. This would then lead to the alleviation of loss of control during flight, as forward swept wings give more control to the pilot through increased airflow on the rear wing-set. Forward swept wings may also reduce the negative impact on the environment created by planes, as forward swept wings may be more efficient than rear swept wings.

Methods

Introduction to Methodology

In this experiment, six models of a wing were 3-D printed because 3-D printing was the most accessible way to obtain customized models. Three of the wings created model forward swept wings and three models represent rear swept wings in order to test the efficiency of both swept wing types. The splitting of model orientations allowed for direct comparison of each sweep orientation. Of the six wing models, two of each were used at differing sweep angles (one sweep angle for each sweep direction). Sweep angles are the angles between the line fuselage/wingtip and the nose of the craft (see Figure 5 – Swept Wing Comparison). The sweep angles used were 15°, 25°, and 35° in order to test the efficiency for a variety of sweep angles. Models were used in order to calculate a preliminary estimate of how efficient forward swept wings are in comparison to rear swept wings (Figures 5, 6, and 7)

Wind Tunnel Design

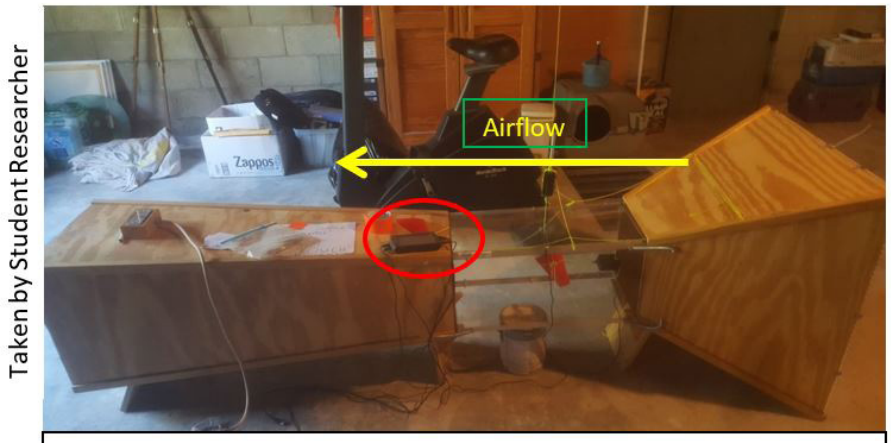

Figure 6: Wind tunnel design. The right-hand side is where the wind tunnel collects air and the left-hand wooden compartment houses the fan. The clear section in the middle is where the models were observed and tested.

Role of Mentor

The role of the mentor in this project was to guide the student researcher through various challenges within the study. For example, the mentor provided important advice in preliminary scaling estimates of model sizes such as the taper angle (severity of diminishing thickness) and chord length (length from wing tip to wing root).

Model Template

Taken by Student Researcher

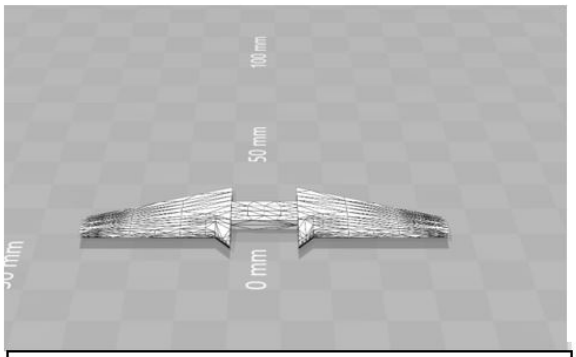

Figure 7: The original template used to create and print the models utilized in this experiment. This was later scaled to better fit the test site

Swept Wing Comparison

Taken by Student Researcher

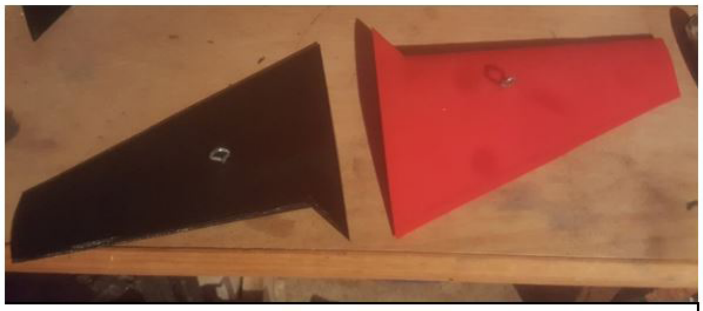

Figure 5: Depicts the comparison between rear (black) and forward (red) swept models.

Materials

This experiment utilized a wind tunnel in order to simulate air moving over a wing. The wind tunnel was borrowed from (and built by) a neighboring district. The wind tunnel was comprised of a long structure with a fan at one end to inhale air create airflow. Air moved from one open side to the other side with the fan creating the airflow at a speed of 8.5 m/s.

This experiment also utilized six different wing models that were designed to simulate swept wings. The models were created using AutoCAD 3-D modeling software. The file template was modified in order to fit the dimensions 12.93 cm x 16.68 cm x 1.61 cm as well as cropped such that there was only one wing printed per model (Fig 4).

I used force sensors to measure the magnitude of the force exerted from the wings that were attached above and in front of the leading edge of the model in order to measure lift and drag. The measurement of lift and drag enabled for calculations determining the efficiency of each model.

There was approximately 50 ft of string and six eye-hooks used in this experiment. This string was what comprised the suspension system and was what allowed the wings to be suspended in the wind tunnel. The string attached to each model on one eye-hook located at the center of balance for each model.

The suspension system's concept arose from the concept of measuring a model's lift and drag values. Contemporary systems often utilize a system that uses a clamp-like structure to hold the model in place. However, the clamp used would dampen the measurements found by the force sensors because the model would have friction on the sides. If the wings were simply floating in the wind tunnel, suspended, then the most accurate readings would be produced. Thereby, the concept of the suspension system was created; the system allows for a more accurate measurement of lift and drag forces as it does not hinder the forces exerted.

Explanation

Suspension System

The suspension system utilized a vertical string attached above the wing model in order keep to the wing model stable in the pitch axis, as well as measure the downward force on the wing. This string also kept the wing model at a constant 25^{o} angle of attack.

Another string was attached to the leading edge of the craft. This line limited yaw (vertical axis) instability as well as measured the frictional force exerted on the wing.

String was also attached to the "Z" axis of the craft, anchored on both sides of the craft. These lines controlled the roll direction of the craft (Figures 8 & 9)

Potential Issues

In this experiment, wing data was gathered twice in order to ensure accuracy as well as expand data points. However, there was some pitch instability in the first dataset. This was caused by the strings controlling the model because they

were only anchored to one point. The second dataset addressed this problem by wrapping the roll string around the wing model. The first dataset will not be used for the calculations of results, as the slight oscillation could have mildly affected results.

Measuring Tools on the Suspension System

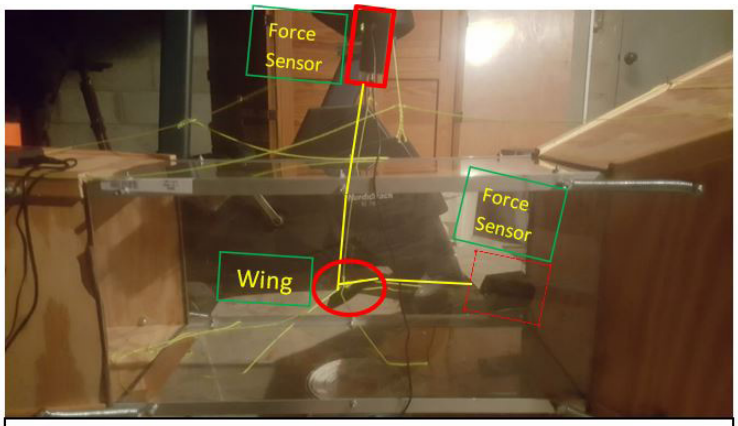

Taken by Student Researcher

Figure 8: Suspension system. The string has the force sensors attached which holds the wing in place. The force sensors and wing model are highlighted with red. The strings that measure lift and drag, by connecting to the force sensors, are also highlighted in bright yellow.

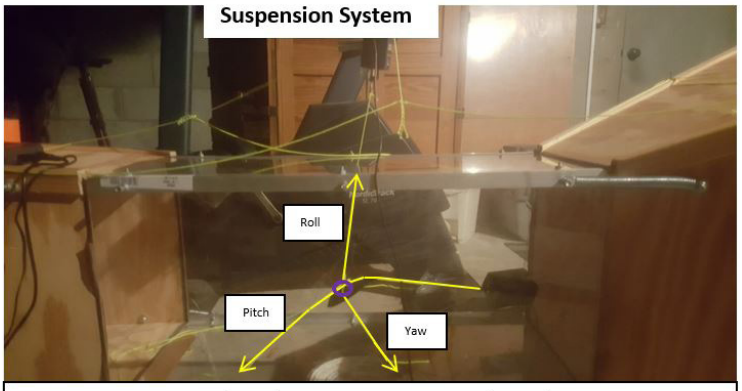

Taken by Student Researcher

Figure 9: Location of each pertinent string. These lines are highlighted in yellow. The strings are labeled by the direction of motion that they control. The purple circle in the middle is an eye-hook connecting the string to the wing.

Data Collection (dataset one)

Force sensors were added to the pitch line attached above the wing as well as the yaw line based from the leading edge of the wing in order to project the magnitude of the force vectors onto a display located near the wind tunnel. The magnitudes could then be recorded for data analysis. Before the wind was turned on, the magnitude for both sensors was recorded. Then, when the wind was turned on, data from each sensor was recorded every two minutes for a total of ten minutes. At the eleventh minute (one minute past when wind was turned off) another reading of force was recorded. This is a similar process to that used in many wind tunnel tests, such as Yu F. Fei and Kuo C. San.[15]

Data Collection (dataset two)

The procedure for dataset two was precisely the same of that for dataset one, except for the wind on total time and the roll string. The wind on total time was doubled to mak twenty minutes with wind. The readings still occurred every two minutes, so the data collected was double when compared to the first data set. The other change with the roll string occurred with the way it was attached. With the second data set, the roll string wrapped around the wing model to give more stability in pitch due to the fact that the string now spanned the length of the wing model, giving more points of

contact to the model and as such stabilizing the movement. The added stability made the data collected more reliable, in terms of calculating efficiency, due to the increased consistency of the data (Figure 10).

Data Analysis

The first step of the analysis process starts with finding the difference in lift and was calculated by finding the average of the downward force (wind on) and subtracting it from the initial downward force (wind off). The equation modeling this calculation is $\mathbf{L = g_i - g_a}$ such that g_a is average gravity (downward force) and g_i is initial gravity. Then, the change in drag must be found by calculating the average of the frictional force (wind on) and then the initial value (wind off)

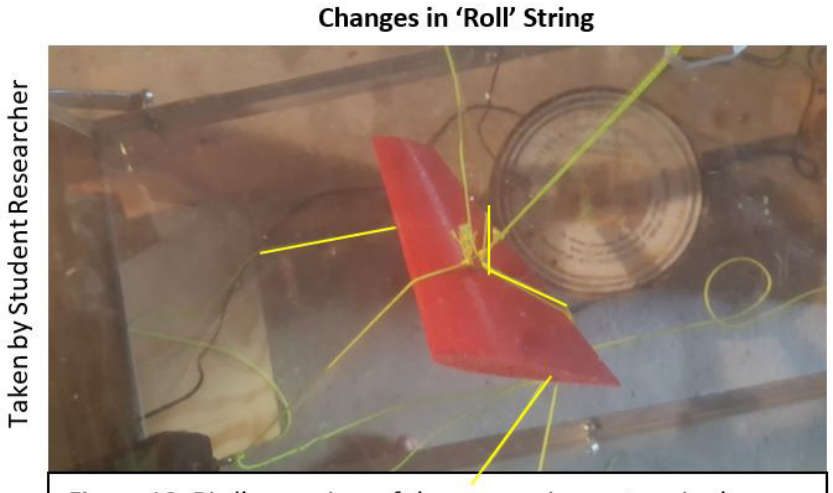

Figure 10: Bird's eye view of the suspension system in the dataset two configuration. The roll string is highlighted and wraps around the model, giving more stability and limiting the resulting oscillation

must be subtracted from this value. The equation $\mathbf{D = d_a - d_i}$ such that d_a is average lateral force and d_i is initial lateral force. Both values (change in lift and drag) should be positive in order to allow easy comparison of the two values making the resulting fraction easier to calculate. After the values of the change in lift and drag are calculated, they are put into a fraction that consists of lift/drag. The equation modeling this ratio is L/D such that L is lift and D is drag. This general efficiency coefficient allows for comparison of every wing tested in this research. A higher value in the lift over drag fraction is equivalent to a general higher efficiency at a given speed and angle of attack, both of which were kept constant in this experiment.

Results and Discussion

Overview

The goal of this research was to test and gather preliminary efficiency values for both forward and rear swept wings. Dataset 1 was not used in order to calculate the efficiency of forward swept wings due to the fact that the wing model oscillated which distorted the force sensor readings. This distortion caused the data collected to not be accurate, as it added extra force to the readings of lift and drag. Dataset 2 concluded that the forward swept wing orientation was more efficient than rear swept wings at 15°, 25°, 35°. Forward swept wings were found to have a higher lift to drag (L/D) ratio at each direct angle comparison (for example: 15° forward swept to 15° rear swept).

Measuring lift

All tables are simplified with the word "Lift" rather than "Gravity" because the lift measurement, for both wind on and off, is actually a measurement of gravity. Lift is then calculated as the difference in gravity, which is then applied to all "lift to drag" values (Table 2).

Lift to Drag Values

The "lift to drag" (L/D) values are what define this experiment. These values are the refined data, calculated through dividing the force of lift by the force of drag, in which efficiency is measured. Each L/D value is calculated from four

values: gravity (lift with wind off), lift (wind on), calibration drag (tension with wind off), and drag (wind on). Utilizing the equations $\mathbf{L = g_i - g_a}$ and $\mathbf{D = d_a - d_i}$, change in lift (Δ lift or L) and change in drag (Δ drag or **D**) were created. These values create the efficiency ratio, defined as L/D.

Lift to Drag Values of Forward and Rear Swept Wings

F-15°	R-15°	F-25°	R-25°	F-35°	R-35°
4.50	2.85	0.96	0.56	0.76	0.80
6.14	2.19	0.90	0.51	1.10	0.78
4.86	2.27	0.94	0.51	1.60	0.82
5.34	1.90	0.95	0.51	1.91	0.82
4.80	1.98	0.92	0.41	2.26	0.85
5.55	1.98	0.88	0.49	3.02	0.80
5.39	1.33	0.87	0.53	3.60	0.86
5.57	2.80	0.90	0.51	3.61	0.86
5.71	2.63	0.84	0.38	3.57	0.82
6.04	1.94	0.85	0.56	3.79	0.81

Table 2: Depicting the lift to drag (L/D) values for each experiment. The headings go by the first letter of the sweep direction followed by the sweep angle. These values were derived from the change in gravity (lift) over the change in drag (in order to compensate for tension).

Average Values

All data gathered is summarized by the average L/D value. These values represent the averaging of all gathered L/D values for each model. In short, these values represent general efficiency of each model and allow for conclusions to be made. If an average L/D value is greater than its comparison, then that model (at 8.5 m/s and angle of attack 25°) is more efficient (Table 3).

Average Lift to Drag Values

	15°	25°	35°
Forward Swept	5.39	.903	2.52
Rear Swept	2.19	.498	.822

Table 3: Each value is the basic average of each L/D value for the model.

Analysis of Data

The data collected indicates that forward swept wings are more efficient than their rear swept counterparts at every tested angle, given the constant angle of attack of 25° due to the fact that the L/D values are higher for forward swept wings. Bonferroni's Multiple Comparison Test showed that almost every comparison between efficiencies was statistically significant. Furthermore, the data shows that forward swept wings are almost twice as efficient as their rear swept counterpart at all tested sweep angles (Table 4).

P Values of Efficiency Comparison

Comparison	Significant
F-15 vs R-15	P<.001
F-15 vs F-25	P<.001
F-15 vs R-25	P<.001
F-15 vs F-35	P<.001
F-15 vs R-35	P<.001
R-15 vs F-25	P<.001
R-15 vs R-25	P<.001
R-15 vs F-35	P>.05
R-15 vs R-35	P<.001
F- 25 vs R-25	P>.05
F-25 vs F-35	P<.001
F-25 vs R-35	P>.05
R-25 vs F-35	P<.001
R-25 vs R-35	P>.05
F-35 vs R-35	P<.001

Table 4: Using Bonferroni's Multiple Comparison Test to statistically compare the average L/D values.

Comparison to Previous Research

This data differs slightly from many other previous studies in the fact that the L/D values were directly compared between forward swept wings and rear swept wings. Previous studies have looked at the efficiency (L/D values) of forward swept wings or rear swept wings, but have never made an issue of pollution by utilizing more efficient wings, the amount of fuel consumed per flight will decrease, thereby most likely leading to a decrease in carbon emissions.

Due to the increased efficiency presented by forward swept wings and due to safety issues, the widespread use of this wing should be implemented. The added control stems from the flow changes forward swept wings provide, leading more air to flow onto the rear wing-set, thereby giving more control to the craft.[16] In addition, this is one of the only studies that focused on the efficiency of forward swept wings.

Review of Goals

The goal of this study was to test efficiency values for both forward and rear swept wings through creating lift to drag ratios and comparing their values at differing angles. This was accomplished by collecting lift to drag ratios for all six models. We determined that forward swept models were more efficient.

Conclusion

This experiment was conducted in order to find the efficiency of forward swept wings and compare them to their rear swept wing counterparts. This was done through the process of suspending 3D models of wings and measuring the lift and drag forces. The readings were then converted into a lift to drag ratio that determined the general efficiency of each model. This experiment found that forward swept wings had a higher lift to drag ratio, and therefore forward swept wings were shown to be more efficient than rear swept wings. If forward swept wings were to be implemented, then aircrafts would decrease the quantity pollutants emitted as well as increase control given to pilots through flow changes. Forward swept wings have the potential to be the most efficient wing type, but they have yet to be perfected.

Acknowledgements

To my parents: Rajesh and Jann Mirchandani
To my teachers: Michael Blueglass and Rachel Koenigstien
To my mentors: Justin Czewiski and Timothy Takahashi

References

1. Iata. “Search.” IATA, 31 Dec. 2013, www.iata.org/pressroom/pr/Pages/2013-12-30-01.aspx
2. Clark, Duncan. “Aviation Q&A: the Impact of Flying on the Environment.” The Guardian, Guardian News and Media, 6 Apr. 2010, www.theguardian.com/environment/2010/apr/06/aviation-q-and-a.
3. Pappas, Stephanie. “Why Private Planes Are Nearly As Deadly As Cars.” LiveScience, Purch, 7 Nov. 2017, www.livescience.com/49701-private-planes-safety.html.
4. “STATISTICS” Accident Statistics, 2017, www.planecrashinfo.com/cause.htm.
5. Walsh, Bryan. “Does Flying Harm the Planet?” Time, Time Inc., 20 Aug. 2007, content.time.com/time/world/article/0,8599,1654488,00.html.

5a. Chris Collins (2007), “Implementing Phytoremediation of Petroleum Hydrocarbons, *Methods in Biotechnology* 23:99–108. Humana Press.

5b. *Chevron Products Corporation. “Aviation Fuels Technical Review”*

6. Essick, Photograph by Peter. “Air Pollution Causes, Effects, and Solutions.” Causes, Effects, and Solutions, 29 Sept. 2017, www.nationalgeographic.com/environment/global-warming/pollution/.
7. Bauer, Matthias, Thomas Grund, Wolfgang Nitsche, and Vlad Ciobaca. “Wing Tip Drag Reduction at Nominal Take-Off Mach Number: An Approach to Local Active Flow Control with a Highly Robust Actuator System” (2016): n. pag. Web.
8. Belyaev, I. V., M. Yu. Zaytsev, and V. F. Kopiev. “Effect of Chevrons on the Slat Noise of Straight and Swept Wings.” Acoustical Physics 61.6 (2015): 715-23. Web.
9. Thomas, Christian, Shahid M. Mughal, Matthew Gipon, Richard Ashworth, and Alejandro Martinez-Cava. “Stability of an Infinite Swept Wing Boundary Layer with Surface Waviness.” AIAA Journal 54.10 (2016): 3024-038. Web.
10. Doig, Graham, Tracie J. Barber, and Andrew J. Neely. “Aerodynamic Characteristics of a Swept Wing in Close Ground Proximity at High Subsonic Mach Numbers.” Journal of Aerospace Engineering 25.4 (2012): 600-12. Web.
11. Tang, Deman, and Earl Dowell. “Experimental Aeroelastic Models Design and Wind Tunnel Testing for Correlation with New Theory.” Aerospace 3.2 (2016): 12. Web.
12. Findanis, N., and N. A. Ahmed. “Flow Studies of a Forward Swept Wing Fitted with Active Flow Control.” (2014): n. pag. Web.
13. Shajanian, Arvin, Timothy Takahashi, Brian German, Matthew Daskilewicz, and Shane Donovan. “Wing Section Thickness and Camber Allocation for Conceptual and Preliminary Aircraft Design.” 49th AIAA Aerospace Sciences Meeting including the New Horizons Forum and Aerospace Exposition (2011): n. pag. Web.
14. Kirkman, Jeffrey J., and Timothy T. Takahashi. “Critical Mach Number Prediction on Swept Wings.”55th AIAA Aerospace Sciences Meeting (2017): n. pag. Web.
15. Yu F. Fei, and Kuo C. San. “Journal of Aerospace Engineering.” Boundary-Layer Flow Effects on Aerodynamic Performance of Forward-Swept Wings | Journal of Aerospace Engineering | Vol 25, Web. 22 Mar. 2017.
16. Hicks, John W., and Edwin J. Saltzman. “In-Flight Lift-Drag Characteristics for a Forward-Swept Wing Aircraft (and Comparisons With Contemporary Aircraft).” NASA Technical Paper 3414 (1994): n. pag. Web.
17. Barrett, James. “Debunking the Jevons Paradox: Nobody Goes There Anymore, Its Too Crowded.” *ThinkProgress*, ThinkProgress, thinkprogress.org/debunking-the-jevons-paradox-nobody-goes-there-anymore-its-too-crowded-7fec531b1411/

Authors

Arjay Mirchandani – A young high school student, Arjay plans on getting a dual major in college, regarding the fields of aerospace engineering and computer programming. He has not chosen which school to attend.

Use of Chitin in Industrial Effluent Plants

Sarah W. Ferdousi[1], Antara Fairu[2]

1. *International Turkish Hope School; Plot: 7, Road: 6, Sector: 4, Uttara, Dhaka-1230, Bangladesh*

[1] *sarahwf77@gmail.com*

[2] *antarafairuz@gmail.com*

Abstract

Chitin is a biopolymer found in abundance all around us: in the cuticles of insects, shells of crustaceans such as shrimp, crabs etc. Many tonnes of shells are produced annually around the world. Bangladesh is a developing country in South Asia. Its much prominent textile industry has resulted in liquid waste being dumped into surrounding water bodies for many years, leading to widespread pollution. Through our study, it has been seen that chitin absorbs heavy metal ions, namely $Pb^{2+,}$ Cd^{2+}, Cu^{2+} and Zn^{2+} which are found in abundance in industrial effluent, ultimately resulting in water which performs better in qualitative and quantitative tests. We intend to introduce chitin as a measure to reduce this pollution through its use in Common Effluent Treatment Plants (CETP) to purify river water as a cheap and environmentally friendly alternative to the harsh chemicals. Chitin can be relatively easily extracted from crustacean shells. We aim to clean the environment, one ion at a time.

Keywords

Chemistry; Bangladeshi rivers; Water pollution; Water purification; Textile; Effluent Treatment Plant (ETP); Chitin; Chitosan.

Introduction

Enormous amounts of chitin can be found in the biosphere; it is the major component of crustacean shells, cuticles of insects, fungal cell walls, yeast and green algae. About 1010-1011 tonnes of annual turnover make it the most abundant as well as the most readily available biopolymer in nature.[1]

In the processing of shrimp for human consumption, between 40% to 50% of the total mass is waste. About 40% of the waste is chitin, incrusted with calcium carbonate and astaxanthin.

About 10% of this waste is dried off to be processed as fish and poultry feed.[2] In developing countries, waste shells are often just dumped in landfills or the sea or incinerated. In developed countries, disposal can be costly — up to US$150 per tonne in Australia,[3] for example. This causes large amounts of pollution in coastal areas and the destruction of marine life.

The utilization of this shellfish waste in the form of chitin to purify a large volume of water would not only prove to be environmentally friendly, but would also, for the above-mentioned causes and costs, be a waste treatment alternative.

Bangladesh is a small country in South Asia, at the apex of the Bay of Bengal. It was deemed the 50th largest export economy in the world. Exports in Bangladesh increased to 230.71 billion BDT in April 2018.[4]

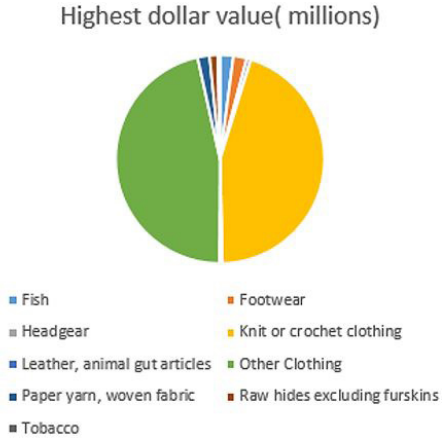

Figure 1. Items making up exports of Bangladesh, and their values

From the statistics listed above, it can be seen that textiles and leather form a large segment of Bangladesh's exports. Despite the significant economic contribution of the textile and leather industries in Bangladesh, it has brought with it a range of environmental problems, mostly pollution of water resources in the country. Most of these industrial units are located along the banks of the rivers, which provide a means of transportation for incoming raw materials and outgoing finished products. Unfortunately, as a consequence, industrial units drain effluents directly into the rivers without any consideration for the environment.

A complex mixture of hazardous chemicals, both organic and inorganic, is discharged into the water bodies from all these industries, usually without treatment. About 33 percent of the industries produces textiles, finished garments or are tanneries, of which the capital, Dhaka, accounts for almost half and Narayanganj about 32%.[5]

a) Textile mill effluent, rich in heavy metal ions, being dumped into a water body, causing a drastic decrease in the quality of life in the area around it.

b) Buriganga river, flowing through the capital Dhaka; overflowing with chemicals used in the tanneries surrounding the river.

c) Despite the government's efforts to reduce pollution with the introduction of new rules and regulations, such waste is regularly being expelled from factories.

A total production of shrimp and fish worth $1,462,843.67 had been exported as of July-December 2016-2017.[6] Shells comprise 40% of the total mass of prawns and are proving to be a matter of concern due to their slow biodegradation.[7] These shells are mostly produced by the seafood processing factories, as well as the frozen food factories as a solid waste. Instead of disposing this waste into the sea, it can be utilized to purify effluent into a much safer alternative— water that is capable of sustaining life.

The goal of our research was to test the effectiveness of chitin extracted in the school laboratory through chemical means from crushed crustacean shells as an adsorbent by subjecting water collected from Buriganga and Turag, the two most highly polluted rivers of Dhaka, to a chitin filter and comparing the pH, turbidity, and iron levels before and after, and researching its sustainability for use in CETP in the long run. This paper differs from similar literature on the same research topic in the respect that it looks into the suitability of chitin for use in CETP in an economy such as that of Bangladesh, both to improve the standard of living and general health.

Methods

The chitin shells were collected from a shrimp processing plant, located in the district of Khulna, in south-western Bangladesh. They were cleaned and dried in direct sunlight for 15 days before further use.

Having cleaned and dried the shells, we roughly milled them (Photo 1). In a jar, we added approximately 40.18g of concentrated sodium hydroxide pellets to a litre of water (1000 mL) for a final concentration of 1.0 mol/dm.[3] After a homogenous solution was made, we added the crushed shells to the solution.

The next step included heating the solution to 60°C for four days straight, with stirring at regular intervals (Photo 2).

Sodium hydroxide was used for deproteinisation (the removal of protein) of the shells. Deproteinisation is necessary because the proteins present may hinder the molecular structure of chitin and its ability to combine with the metal ions.

The shells turned a slightly brighter shade of orange than prior to treatment, while the solution turned an olive green-orange colour (Photo 3).

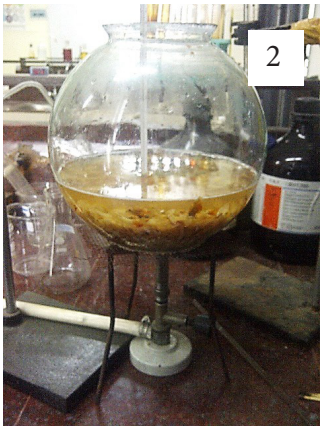

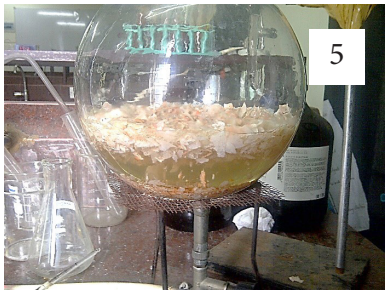

After four days, we removed the solids from the solution (Photo 4), washing with distilled water and drying them again, before immersing them into a solution of concentrated hydrochloric acid, of concentration 2.0 mol/dm^3. We kept the crushed shells in this solution for two days (Photo 5).

The demineralization process (Photo 5, Photo 6, Photo 7), can be performed with acids such as HCl, HNO3, H2S04, CH3COOH and HCOOH. Especially, hydrochloric acid seemed to be the preferred reagent in the case of chitin-containing waste materials. The demineralization process is done to reduce the content of mineral substances in tissue or organism, so that they become mineral-deficient. This enables them to regain the lost minerals (metal compounds) from effluent.

Lastly, we treated the carapaces, now weighing 153.4 g, in an organic mixture of chloroform, methylated spirit and water, in the proportions 1:2:4. This was done for elimination of pigments, lipids and decolourisation for four hours. Finally, the rest of the sample was dried within a drying oven at 60°C for 48 hours and then weighed to determine the chitin contents.

The lab-prepared chitin was subjected to two separate tests: one involving purifying a sample of water containing zinc, iron, chromium, prepared in the lab beforehand, made to replicate the polluted water, the second involving water collected from the Turag river. The model factory used in the project had a two-stage purification process for the discharge going into the water bodies. The primary stage consisted of the chitin crushed into minute particles and compressed into a filter; the secondary stage had clean coarse red sand, used to remove pathogens.

Results and Discussion

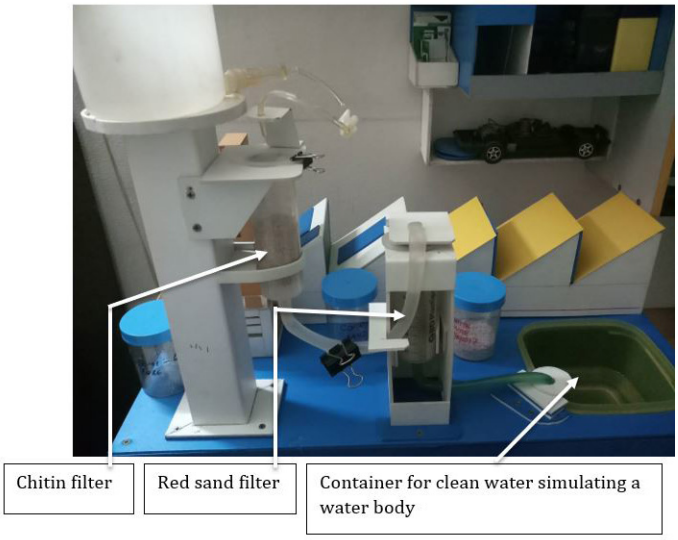

Figure1: A scaled-down model of the proposed ETP using a chitin filter

The filtered water was subjected to three tests:

- A turbidity test, using a Hach 2100Q turbidimeter
- A qualitative test for iron, using a Hach Iron Colour Disc Test Kit
- A test for the pH, using universal indicator

Table 1. Change in turbidity

Turbidity	
Before being passed through chitin filter/ NTU	After being passed through chitin filter/ NTU
101	1

Table 2. Change in iron levels

Iron Levels	
Before being passed through chitin filter	After being passed through chitin filter
	

Table 3. Change in pH

pH	
Before being passed through chitin filter	After being passed through chitin filter
8	7

The water collected from the container as shown in the diagram, after being passed through both the filters shows drastic improvements in turbidity, iron levels and pH. This proves that chitin is effective in elevating the quality of effluent to a level safe enough to be released into water bodies and is therefore ideal to be used in ETPs.

Although this process is easier and faster, there are a number of problems that this method poses:

- Harsh chemical treatments may result in hydrolysis of the polymer, and different structural inconsistencies.
- This method may be energy consuming, and the remaining solution may be a source of pollution.
- The protein components may no longer be useful as animal feed.[2]

Therefore, we propose the alternative biological method for large scale production for industrial use.[2] The alternative method is carried out by treating the sun-dried shells with protease-producing bacteria, the enzyme produced results in deproteinisation, thus avoiding alkali treatment. Deproteinisation mainly occurs through the added lactobacillus, or the gut bacteria of the shrimp, if raw fish has been used. Demineralization can be achieved through the lactic acid produced by bacteria through the conversion of an added carbon source. This method ensures homogeneity of the final product as well as high quality. The approach allows for obtaining a liquid fraction rich in proteins, minerals and astaxanthin and a solid chitin fraction. The liquid fraction can be used either as a protein-mineral supplement for human consumption or as an animal feed. It is affordable, since it is neither energy nor capital intensive, and has the increased efficiency of the procedure.

Conclusion

The importance of chitin lies in its biological (biodegradability, biocompatibility and non-toxicity) properties.[2] The use of chitin in effluent treatment plants in Bangladesh can be justified since water pollution in Bangladesh has exceeded danger levels since as early as the 1980s. According to the Dhaka Water and Sewerage Authority (WASA), about 12,000 cubic metres (420,000 cu ft) of untreated waste are released into rivers from Tejgaon, Badda and Mohakhali industrial areas every day.[8] Nearly four million people in the city are exposed to the consequences of water pollution on a daily basis. Meanwhile, the waste from flourishing seafood processing factories, disposal of which can prove to be quite cumbersome, can be turned into chitin to be used in CETPs, effectively producing water that is suitable to be released into the water bodies of Dhaka. Use of chitin will not only take care of the waste problem, but will drastically improve the lives of thousands of people who depend on these water bodies. It is thus sustainable in the long-run.

Acknowledgements

We would firstly like to thank our Chemistry teacher, Ms. Menekse Tok, for not giving up on us, and constantly looking out for opportunities and platforms for us to present this project. She has been a source of inspiration and encouragement for us. We would also like to thank our Physics teacher, Md. Imran Khan, and Mathematics teacher, Mirza Md. Ragib, for going through this paper and for their advice and kind words; our school, ITHS, for allowing us the freedom to perform the experiment in the laboratory at our own pace, and for providing us with the necessary equipment.

A special thanks to our friends for not letting us give up, and for their constant supply of anecdotes and smiles; our parents, for their love and support for each and every step we have taken.

Last but not the least, we would like to extend our gratitude to Abdul Kalam Azad for providing us with the crab shells.

References

1. G.W. Gooday et al., Mineralization of Chitin in Estuarine Sediment, 1991.
2. W. e. a. Arbia, “Chitin Extraction from Crustacean Shells Using Biological,” 2012.
3. Lakka, Sajani S, and Jasti S Rao. Antiangiogenic Therapy in Brain Tumors. Oct. 2008, www.ncbi.nlm.nih.gov/pmc/articles/PMC2656359/?report=reader.
4. Jain, Rakesh K, et al. Angiogenesis in Brain Tumours. Aug. 2007, www.bing.com/cr?IG=5B991BCBC1684E558CDEAF6E00E8611C&CID=1121BE06595E6F2F32BDB59A58F16E4D&rd=1&h=4nGCkR7uAkoADkSYHs78LdFydVRK-71eku0qO8njpeI&v=1&r=http%3a%2f%2fwww.nature.com%2fnrn%2fjournal%2fv8%2fn8%2fabs%2fnrn2175.html&p=DevEx,5072.1.
5. “Angiogenesis Inhibitors.” National Cancer Institute, www.cancer.gov/about-cancer/treatment/types/immunotherapy/angiogenesis-inhibitors-fact-sheet.
6. Vasudev, Naveen S., and Andrew R. Reynolds. Angiogenesis, Springer Netherlands, 2014, www.ncbi.nlm.nih.gov/pmc/articles/PMC4061466/.
7. Ackerman, Rachel, et al. “SLT-VEGF Reduces Lung Metastases, Decreases Tumor Recurrence, and Improves Survival in an Orthotopic Melanoma Model.” MDPI, Molecular Diversity Preservation International, 27 Aug. 2010, www.mdpi.com/2072-6651/2/9/2242.
8. Hotz, Birgit, et al. Neoplasia (New York, N.Y.), Neoplasia Press Inc., Oct. 2010, www.ncbi.nlm.nih.gov/pmc/articles/PMC2950329/.

Authors

Sarah Wasifa lives in the sketches of a dream where her love for physics helps revolutionize the way one looks at the world and its many tales.She wants to major in subjects related to quantum physics, namely particle physics, all the while nurturing her fervent love for creative writing. She intends to pursue higher education at the Harvard John A. Paulson School of Engineering and Applied Sciences.

Antara Fairuz has a world full of creativity in her head along with dreams of discovering ways to cure diseases and make this world a better place. She wants to major in subjects related to medicine and biomedical sciences, preferably genetic and biomedical engineering. She intends to pursue higher education at Harvard John A. Paulson School of Engineering and Applied Sciences.

Study of Carbon Nanotube Epoxy Resin Coated Carbon Unidirectional Fiber Fabric in Radiation Shielding

Kaylee M. Cunningham

1. Olympic Heights Community High School, 20101 Lyons Rd, Boca Raton, FL, 33434, USA

kayleecunningham@ufl.edu

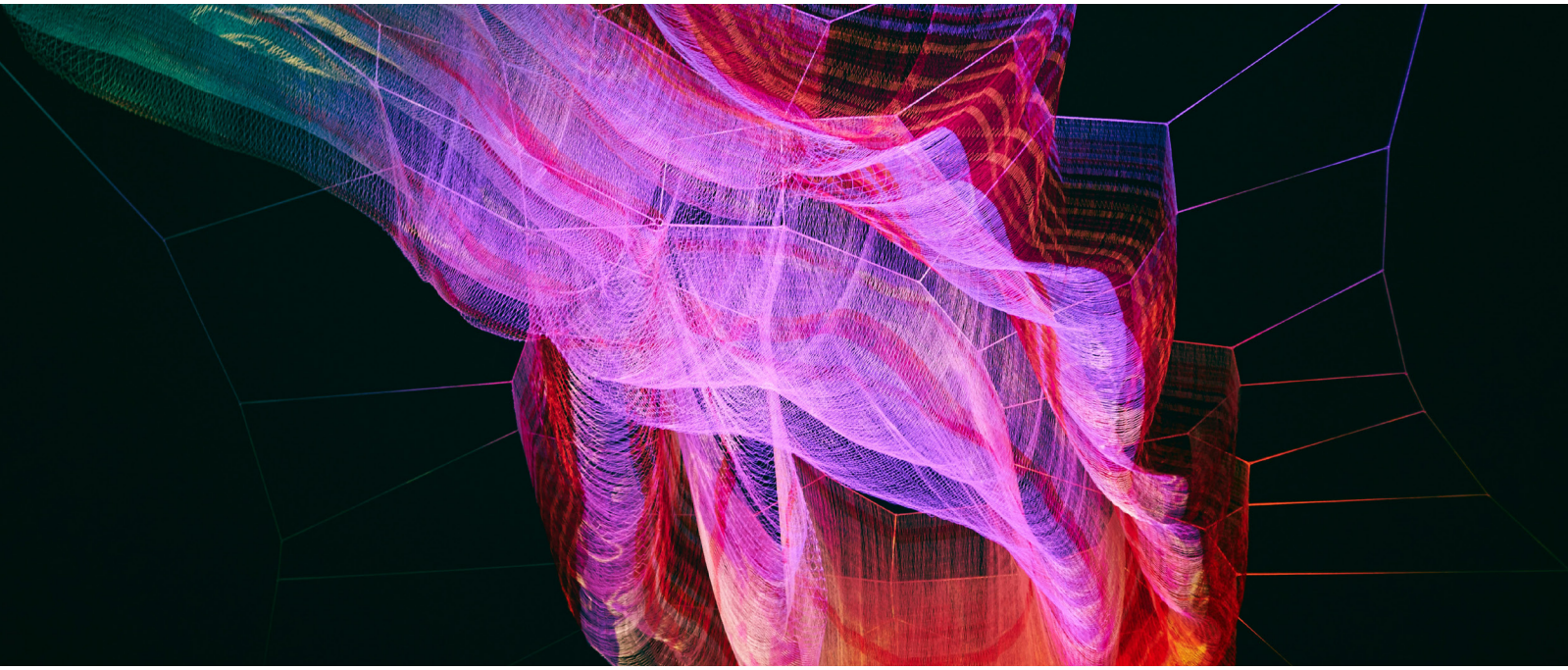

Abstract

This experiment was conducted in an effort to advance technology used to better protect humans from ionizing gamma radiation, emitted from a small uranium-235 sample encased in glass. The goal in performing this study was to determine if carbon nanotube epoxy resin coated carbon unidirectional fabric would prove effective in reducing the amount of ionizing radiation that would penetrate a normal cotton bra. Carbon nanotube epoxy resin is epoxy infused with small, graphite-like tubes. Carbon unidirectional fiber fabric is material made out of carbon fibers woven parallel to each other. Carbon's crystal-lattice molecular structure makes it naturally strong. By creating nanotubes out of this material, it becomes lightweight and remains strong and highly conductive; thus, a combination of carbon nanotube epoxy resin and carbon fiber fabric was predicted to shield radiation. The carbon fibers and carbon nanotubes reflect radiation, while the polymers of the epoxy absorb radiation. To test this, an ionization chamber was built out of a soup can to measure changing voltage through various materials: a test was performed with no cover to collect a control reading, aluminum foil, cotton, and carbon nanotube coated carbon unidirectional fabric were tested. The ionization chamber measured a 44% radiation reduction for the encased uranium sample. For more accurate results, the experiment was reconducted with a Geiger counter. The experiment was replicated and included testing a double-layer carbon unidirectional fabric coated in carbon nanotube epoxy resin, as well as an uncoated piece of carbon unidirectional fabric. Consequently, carbon unidirectional fiber fabric alone resulted in a 33% radiation penetration reduction. The single layer fabric resulted in a 55% radiation penetration reduction. The double layer fabric resulted in a 72% reduction rate. The foil had a 7% reduction, the cotton fabric had a 14% reduction, and the uncoated fabric had a 33% reduction. According to these results, the carbon nanotube epoxy resin coated carbon unidirectional fiber fabric was effective in significantly reducing radiation penetration rates.

Keywords

Nanotechnology; Carbon Nanotubes; Epoxy; Radiation; Shielding

Introduction

Radiation poisoning is an up-and-coming problem in today's technologically advanced society. From nuclear meltdowns like Fukushima, to deep space travel, to radon gas in basements, we are finding ourselves as a species more frequently exposed to various types of harmful ionizing radiation. In particular, flight attendants, nurses, and astronauts are at increased risk of developing cancer caused by radiation exposure. Through this experiment, I aim to contribute to the prevention of breast cancer specifically by developing a fabric to be used in sports bras that reduces dangerous exposure.

Carbon fibers are defined by Merriam-Webster Dictionary[1] as "a very strong lightweight synthetic fiber made by carbonizing acrylic fiber at high temperature." Numerous studies have been conducted and show the effectiveness of carbon fiber in deflection radiation, such as one conducted by Brookhaven National Laboratory[2] where high energy proton beams fired at a carbon fiber reinforced metal were deflected. Likewise, a carbon nanotube is defined as a tube-shaped molecule made up of many of carbon atoms[1]. Carbon nanotubes look almost like rolled up, nanoscopic chicken wire. They can be single walled, or multi-walled, meaning they can be one tubular shape, or multiple tubes stacked.

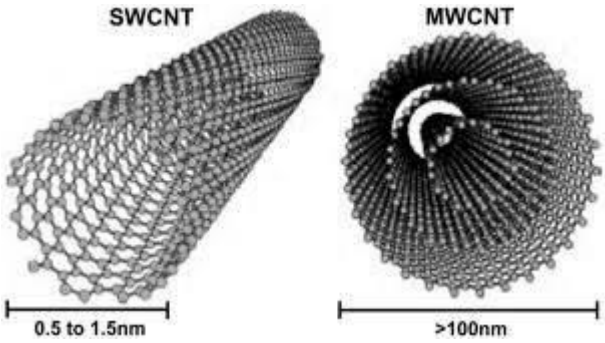

Figure 1 A visual depiction of single walled carbon nanotube (SWCNT) vs multiwalled carbon nanotube (MWCNT).[3]

Several studies have demonstrated that carbon nanotube infused materials have been proven effective in reducing the impact of radiation penetration.[4] Carbon materials are generally effective in reducing radiation penetration because of the strong, conductive, and reflective properties of carbon.[5] By creating nanotubes out of this material, it becomes lightweight and remains strong after radiation exposure, which tends to deteriorate and weaken most metals. NASA currently uses carbon nanotubes in nuclear reactors to prevent metals from deteriorating. This experiment was performed to determine whether the nanotubes actually reflect some of the ionizing radiation. The researcher predicts single-walled carbon nanotube epoxy coated carbon unidirectional fiber fabric will decrease radiation penetration rate. Through experimentation, the researcher hopes to design a fabric-like material that reduces radiation penetration by combining both carbon fiber and carbon nanotubes. The researcher hypothesizes that if she coats unidirectional carbon fiber fabric in carbon nanotube epoxy resin, then radiation will not penetrate heavily through the material, thus protecting against radiation.

Methods

Procedure:

I laid one sheet of unidirectional carbon fiber fabric (available online at sollercomposites.com)[6] on a towel. I then poured a quarter-sized drop of carbon nanotube epoxy resin (also available at sollercomposites.com)[7] onto the top of the fabric and spread it evenly. I left the coated fabric to dry for approximately 1 hour. I then flipped the fabric over and coated the other side and hung it to dry for 24-48 hours.

I built the ionization chamber using the following schematic:

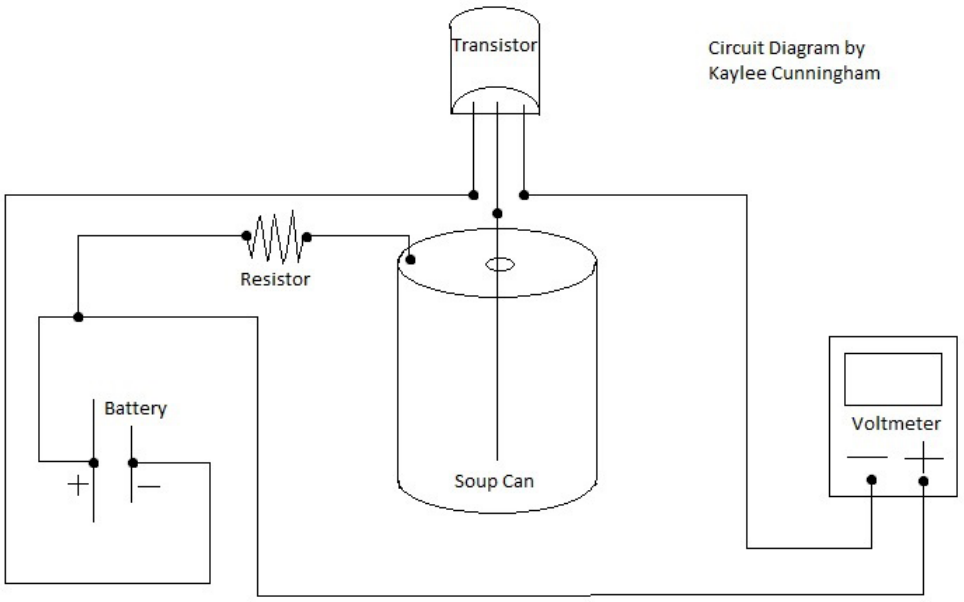

I started by peeling any wrapper off the soup can and thoroughly washing out the inside.[8] I used a thumbtack to poke a small hole in the bottom of the soup can. I poked a nail through the hole to widen it. I spread apart the three prongs of a transistor. I bent the middle prong downward and the left to the left, the right to the right. I soldered the uninsulated wire to the middle prong of the transistor. I soldered the insulated wire to each of the other two prongs (the left and the right). I then threaded the uninsulated wire through the hole in the soup can, ensuring it did not actually touch the can. I taped the top black part of the transistor to the bottom of the can, ¼ cm above the hole. I then soldered one end of resistor to the left of the bottom surface of the can, leaving the other end hanging off the can. After, I soldered the end of left insulated wire to the negative battery connector wire. I connected the negative end of voltmeter to the right insulated wire and coiled the wire around the negative voltmeter lead. Then, I connected the positive end of the voltmeter to the free end of the resistor and coiled the end of the resistor around the positive voltmeter lead. I soldered the positive battery connector wire to the resistor above the connection to the voltmeter. While wearing gloves, I placed uranium glass beads (available at madscientisthut.com for legal purchase under NRC regulations)[9] under the open top of the can. I recorded the voltage (control). I covered the open top of the ionization chamber with aluminum foil and a rubber band. I again recorded voltage. I repeated this with cotton fabric as a cover, and carbon nanotube epoxy coated carbon fiber fabric as a cover for three trials.

Radiation Represented in Voltage				
Trial Number	No Cover (V)	Foil (V)	Cotton (V)	Carbon Nanotubes (V)
Trial 1	5.74	5.69	5.32	3.22
Trial 2	5.76	5.72	5.3	3.18
Trial 3	5.76	5.71	5.34	3.19
Averages	5.75	5.71	5.32	3.20
% Penetration	100%	99%	92%	56%
% Reduced	0%	1%	8%	44%

For further testing with the Geiger counter, I laid two sheets side by side of unidirectional carbon fiber fabric on a towel. I coated two pieces of fabric. Before the resin on each dried, I placed one fabric on top of the other, with both coated sides touching. I allowed it to dry for one hour, then coat the top and bottom of the combined piece of fabric. I left the double layer fabric to dry for 24-48 hours. I then labeled the different types of fabric as “not coated,” “coated single layer,” and “coated double layer.” I laid out an aluminum foil square and cotton t-shirt square on the newspaper in line. On the towel, I laid out the not coated, coated one- piece, and coated two-piece fabrics in line.

Using the ruler, I measured two inches from the bottom of the cup. I cut straight down from the top of the cup to the two inches marked line. From there, I cut around so that I created a miniature cup. I opened the bag of uranium infused glass beads. I poured the beads into the small cup. I counted the beads and recorded the number. I placed the cup of beads on the newspaper, below my line of fabrics. Using a screwdriver, I carefully unscrewed the four

screws on the back of the Geiger counter, in order to expose the Müller tube to remove any possible shielding from the plastic backing of the device for more accurate readings. I collected the screws and screwdriver in the Geiger counter box to prevent losing them.

With no cover over the small cup of uranium infused glass beads, I held the Müller tube of the Geiger counter directly over the cup for one minute and recorded the highest CPM reached (to include the most amount of radiation that penetrates the material) in one minute (to standardize time and allow for the Geiger counter to adjust). I then placed the aluminum foil sheet over the top of the cup and held the Müller tube of the Geiger counter directly over the cup for one minute. I recorded the highest CPM reached in one minute. I replaced the aluminum foil sheet with the sheet of cotton fabric and held the Müller tube of the Geiger counter directly over the cup for one minute. I recorded the highest CPM reached in one minute. I replaced the sheet of cotton fabric with the sheet of not coated carbon unidirectional fabric and held the Müller tube of the Geiger counter directly over the cup for one minute. I recorded the highest CPM reached in one minute. I replaced the sheet of not coated carbon unidirectional fabric with the coated one-piece fabric and held the Müller tube of the Geiger counter directly over the cup for one minute. I recorded the highest CPM reached in one minute. I replaced the sheet of coated one-piece fabric with the coated two pieces fabric and held the Müller tube of the Geiger counter directly over the cup for one minute. I recorded the highest CPM reached in one minute and repeated for 20 trials.

Radiation Represented in Clicks Per Minute (CPM)						
Trial Number	No Cover	Foil	Cotton	CUF	1 Layer CNCF	2 Layer CNCF
1	89	83	75	60	44	26
2	93	88	80	64	38	28
3	92	86	79	62	44	26
4	95	90	80	61	45	25
5	93	88	81	65	41	28
6	91	85	80	60	40	24
7	93	86	81	64	42	27
8	90	86	81	62	40	28
9	92	87	80	63	45	25
10	92	86	79	60	39	25
11	93	86	81	61	40	26
12	92	87	80	62	41	25
13	94	84	81	62	43	25
14	94	87	79	63	42	24
15	95	86	78	62	40	27
16	94	84	80	60	40	26
17	92	86	82	64	43	24
18	90	87	81	64	45	27
19	95	84	80	63	44	26
20	91	86	80	62	43	25
Averages:	93	86	80	62	42	26
% Penetration:	100%	93%	86%	67%	45%	28%
% Reduced:	0%	7%	14%	33%	55%	72%

Results

The soup-can ionization chamber data is not completely reliable because the chamber was never calibrated to a radiation measurement standard. Radiation is commonly measured in counts per minute (cpm) or microsieverts (uSi). The radiation detected by the chamber was measured in change in voltage. The data collected from the chamber demonstrates that carbon unidirectional fabric coated in carbon nanotube epoxy resin is 38% more effective than cotton in preventing radiation penetration, as 92% of radiation penetrated the cotton and only 56% penetrated the carbon unidirectional fabric coated in carbon nanotubes (44% reduction). Percentages were determined by dividing an average shielded radiation value (i.e. covering the chamber with aluminum and obtaining an average reading of 5.7 Volts) into the average unshielded radiation value (i.e. the average value obtained with no cover over the chamber) and multiplying by 100. After testing with a reliable, calibrated Geiger Counter, the researcher was able to determine that the single layer fabric actually penetrated by 45% (55% reduction). However, after testing a double layer of fabric, only 28% of radiation penetrated (72% reduction). In comparison, the uncoated carbon unidirectional

fabric allowed for 67% penetration (33% reduction), while the cotton fabric resulted in 86% penetration (14% reduction), the foil resulted in 93% penetration (7% reduction) and the uncovered uranium infused glass beads were used as a control, measuring 100% penetration (0% reduction). With this data, the researcher performed a paired t-test to determine statistical significance. In comparing cotton with carbon unidirectional fiber fabric, the researcher calculated a p-value of 6.158 x 10-22. Since this value is significantly below 0.05, it can be determined that the data is statistically significant, meaning it did not occur coincidentally. In comparing cotton with two-layer carbon nanotube epoxy coated carbon unidirectional fiber fabric, the researcher calculated a p-value of 3.575 x 10-29. Next, the researcher washed the material to determine if it would be affected by it, as all clothing must eventually be washed. After washing the material inside the sports bra padding and repeating the procedure, the researcher discovered a 1% increase in radiation penetration in the left pad and a 2% increase in radiation penetration in the right pad. Although this may indicate pad deterioration, it may also be due to human error. To determine whether the material actually deteriorated, the material must be washed and tested for more trials.

Discussion

Because the measurements using the ionization chamber were not standardized, without a proper Geiger counter, the accuracy of the chamber cannot be determined. Likewise, because the chamber was built out of old parts by a researcher not well versed in electronics, a large margin for human error exists. Thus, the chamber data is somewhat unreliable.

Overall, the material may be used as a more efficient alternative to lead vests that must be worn during x-rays, should it be further tested with more accurate equipment.

Likewise, it could also be perhaps utilized as a layer of protection in astronaut suits. As we continue to explore space, we must take into account cosmic radiation.

Ideally, the researcher would like to use the fabric as a layer in sports bras, so as to reduce radiation exposure to breasts, and ultimately reduce development of breast cancer. If the material is molded to the shape of a breast, then it should hold as a comfortable layer of padding. The researcher plans to develop and sew a prototype sports bra with a layer of the double layered carbon nanotube epoxy coated carbon unidirectional fabric inside. As the carbon fabric is inexpensive and lightweight, it may prove to be an effective layer in sports bras. The overall goal is to design and produce an effective radiation reducing sports bra to sell at an affordable price to women working in high-risk environment—particularly nurses frequently exposed to X-rays or ionizing particles from radiation therapy, flight attendants frequently exposed to cosmic radiation, astronauts, or nuclear engineers. It will serve essentially as an extra layer of protection. Like the use of sunscreen, which can still result in a sunburn, this garment will not guarantee the wearer will not get breast cancer. It works merely as a preventative garment.

In the future, the researcher hopes to conduct a study in which flight attendants and radiologists wear the garment as an extra layer of protection over a period of 10-15 years, evaluating how many develop breast cancer in comparison to a similar group who did not wear the garment, to reveal the efficacy of the bra as a solution to preventing the development of breast cancer.

Conclusion

This experiment was conducted in order to further technology used to better shield people from radiation. The researcher's goal in executing this experiment was to decide if carbon nanotube coated carbon unidirectional fabric would be effective in reducing the amount of ionizing radiation that passes through fabric. This was tested by building an ionization chamber out of a soup can to study changing voltage through several materials: no cover, aluminum foil, cotton, and carbon nanotube coated carbon unidirectional fabric. The ionization chamber measured a 44% reduction in radiation penetration. To improve the accuracy and reliability of the experimental data, the researcher proceeded to re-conduct the experiment with a Geiger counter. The testing was replicated with the addition of experimenting with a double-layer carbon unidirectional fabric coated in carbon nanotube epoxy resin, as well as an uncoated piece of carbon unidirectional fabric. The single layer fabric resulted in a 55% radiation penetration reduction. The double layer fabric resulted in a 72% reduction rate. The foil resulted in a 7% reduction, the cotton fabric managed a 14% reduction, and the uncoated fabric had a 33% reduction. According to these results, the ionization chamber was not completely accurate, but it was not drastically far off. After conducting the experiment, the researcher performed a paired T-Test to further analyze the data, specifically for statistical significance. It turns out the data is extremely statistically significant, as the set's p-value in comparing cotton vs. carbon unidirectional fiber fabric is 6.158x10-22. The p-value in comparing cotton vs. carbon nanotube epoxy resin coated carbon unidirectional fiber fabric is 3.575x10-29. In the future, the researcher plans to continue researching to determine exactly how effective the

material is in preventing the development of cancerous tumors. Following such testing, should the newly collected data be proven accurate, the researcher plans to start a business using the double layer fabric as a layer in sports bra padding, so as to reduce ionizing radiation exposure and work as a preventative measure for women working in high-risk environments, generally aiming to diminish breast cancer development.

Acknowledgements

I acknowledge my parents for their support in my conducting research at home, as well as Ms. Nimmi Arunachalam, Ms. Deborah Posner, and Ms. Kelly Lawrence for their constant support and encouragement in each and every one of my endeavors.

References

1. Carbon Fiber. (n.d.). Retrieved from https://www.merriam-webster.com/dictionary/carbon fiber
2. Simos, N., & Zhong, Z. (2016, November). Radiation damage and thermal shock response of carbon-fiber-reinforced materials to intense high-energy proton beams. Retrieved from Radiation damage and thermal shock response of carbon-fiber-reinforced materials to intense high-energy proton beams
3. K. (2017, June 19). Carbon Nanotubes (CNTs). Retrieved from https://kailashafoundation.org/2017/05/20/carbon-nanotubes-cnts/
4. Kovo, Y. (2015, February 20). Radiation Shielding Systems Using Nanotechnology. Retrieved September 15, 2017, from https://www.nasa.gov/ames-partnerships/technology/technology-opportunity-radiation-shielding-systems-using-nanotechnology
5. Carbon - Element information, properties and uses | Periodic Table. (n.d.). Retrieved from http://www.rsc.org/periodic-table/element/6/carbon
6. Soller Composites. (n.d.). Carbon Fiber MSDS. Retrieved October 2, 2017, from http://www.sollercomposites.com/MSDS/CarbonMSDS.htm
7. Soller Composites. (n.d.). Carbon Nanotube Epoxy Resin MSDS. Retrieved October 2, 2017, from http://www.sollercomposites.com/images/820%20NanoResin.pdf
8. B. (2011, May 08). How to build a Geiger counter / radiation detector from household materials. Retrieved September 15, 2017, from https://www.youtube.com/watch?v=cfVBW622Vbs&t=5s
9. § 40.13 Unimportant quantities of source material. (n.d.). Retrieved October 10, 2017, from https://www.nrc.gov/reading-rm/doc-collections/cfr/part040/part040-0013.html

Authors

Kaylee Cunningham is a recently graduated senior from Olympic Heights Community High School in Boca Raton, FL. She placed fourth in the Materials Science Category for this research project at the 2018 Intel International Science and Engineering Fair. She will be attending the University of Florida fall 2018 to study Nuclear Engineering.

Evaluation of Recombinant Cytotoxins for the Therapy of CNS Tumors in Experimental Mouse Models

Shrila T. Shah

1. Yorktown High School, 3061 Chen Court, Yorktown Heights, New York, 10598, USA

shrila.shah@yorktown.org

Abstract

Malignant brain tumors, continue to be the cause of a disproportionate level of mortality, killing over 17,000 people each year. For metastasis, blood vessels are constructed (angiogenesis) to provide cancerous tissue with nutrients/oxygen. Blocking this would prevent the supply of factors essential for tumor growth. Angiogenesis is controlled by a balance of pro and anti-angiogenic factors in endothelial cells. Vascular endothelial growth factor (VEGF) is a key proangiogenic molecule that can be targeted with small molecule inhibitors such as Sunitinib, which have demonstrated, with some success, down regulation of tumor angiogenesis. However, benefits are often transitory, followed by restoration of tumor progression. The goal of this study was to determine if introducing an SLT-VEGF fusion protein would selectively target VEGFR-2 being overexpressed in vasculature, preventing “rebound” of vessel angiogenesis. SLT-VEGF is comprised of the subunit A Shiga-like toxin, which binds to VEGFR-2, inhibiting protein synthesis in cells. Cell lines glioma and glioblastoma were grown in flanks of nude mice as model systems to analyze the effects of treatment with Sunitinib (followed by growth without treatment), and SLT-VEGF (followed by growth without treatment). Cyrosections were prepared for immunohistochemical staining to assess the degree of angiogenesis. Results showed that SLT-VEGF treatment significantly blocked the rebound of new blood vessel formation around the tumor.

Keywords

Medulloblastoma; Angiogenesis; Sunitinib; Shiga-like Toxin; VEGFR-2; CD31; cyrosections; immunohistochemical

Introduction

About 80,000 new cases of primary brain tumors are diagnosed annually in the United States and approximately 32% of these tumors are malignant. This year, it is anticipated that nearly 17,000 people will die from a primary malignant central nervous system tumor of one form or another. Glioblastomas, which are a subtype of gliomas that arise from the supportive tissue of the brain, are one of the most common and aggressive brain tumors with about 12,390 new cases expected this year.[1] The prognosis for glioblastoma patients is still poor with a median survival time of 15 months despite current treatment approaches. Conventional methods include: surgical resection, radiotherapy, and chemotherapy.[2] Unfortunately, these therapies are often not effective in treating glioblastomas and they have long-lasting adverse effects, including impaired neural development (especially for children). Specifically, radiation therapy causes late effects such as neurocognitive deficiencies, hormone deficits, and growth impairment. The most common chemotherapy-related late effects are ototoxicity caused by platinum drugs, secondary leukemia, and infertility following exposure to alkylating agents.[3] Therefore, since present therapy is relatively ineffective in treating this disease and puts the surviving patient at risk of severe side effects, a less toxic and more effective therapy is needed.

Angiogenesis in Tumor Growth

One current alternative treatment researched focuses on inhibiting the process of angiogenesis. Angiogenesis, the formation of a vascular network, is necessary for tumor formation in solid malignancies. As shown in figure 1, a tumor mass requires blood vessel networks to provide it with oxygen and metabolites in order to grow. This angiogenic process is far from simple, as it involves a multitude of interacting factors whose final outcome is determined by the balance of the pro- and anti-angiogenic factors produced by the tumor cells. It is seen that the 'angiogenic switch' is 'turned off' when the effects of proangiogenic molecules are balanced by that of anti-angiogenic molecules, and it is 'turned on' when the net balance is in favor of angiogenesis.[4] Further studies have shown that vascular endothelial growth factor (VEGF) is a key driver of angiogenesis. One main VEGF receptor, VEGFR-2, is commonly overexpressed on the vasculature of most solid cancers including glioblastomas. As illustrated in Figure 2, an inhibition of VEGF-driven tumor angiogenesis has been shown to suppress tumor growth in animal models.[5] Thus, given the characteristic high degree of endothelial proliferation, vascular permeability and ubiquity of proangiogenic growth factors, the targeting of blood vessels in brain tumors is a particularly attractive therapeutic strategy.

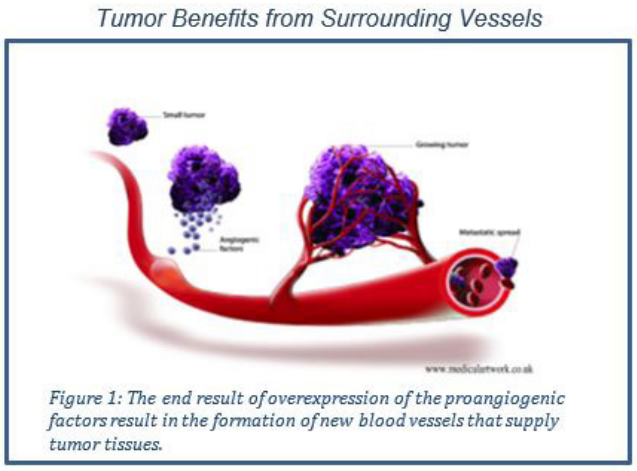

Figure 1: The end result of overexpression of the proangiogenic factors result in the formation of new blood vessels that supply tumor tissues.

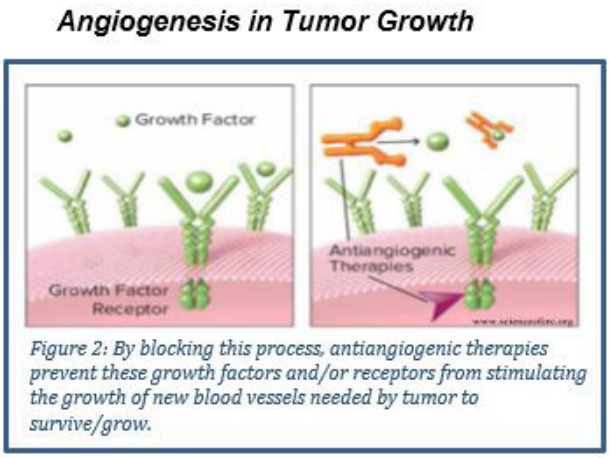

Figure 2: By blocking this process, antiangiogenic therapies prevent these growth factors and/or receptors from stimulating the growth of new blood vessels needed by tumor to survive/grow.

Mechanisms of Response and Resistance to VEGF-targeted Therapy

Today, there are two main strategies to target the tumor vasculature; anti-angiogenic drugs aimed at preventing the process of angiogenesis, thus stopping the formation of new blood vessels that are necessary for the growth and progression of the tumor and metastasis; and an antivascular therapy targeted to the already existing tumor vasculature.[5] Although anti-angiogenic therapies such as Bevacizumab or Sunitinib have been shown to be successful in inhibiting the growth of tumor associated blood vessels, recent studies have demonstrated several important problems with these treatments.[6] One of the most prominent issues is the development of resistance to anti-angiogenic therapy that most likely explains the varying results obtained in these studies. Resistance can essentially be broadly classified into inherent resistance, where the tumors fail to respond from the beginning of a treatment and acquired resistance, where tumors initially respond and then progress while still on treatment. Since anti-angiogenic therapy targets tumor cells indirectly by acting on tumor blood vessels, mechanisms that determine its response and resistance are likely to stem from a complex interaction between tumor cells. Acquired resistance

may perhaps occur because the tumor finds an alternative means to drive tumor vascularization and therefore is insensitive to the therapy, or because tumor cells become adapted so that they can grow despite the reduced vascular supply.[7] Although inhibitors of VEGF/VEGFR signaling were expected to inhibit tumor growth via inhibition of endothelial cell proliferation, experimental evidence indicates that it induces vascular regression, presumably by inhibiting pro-survival VEGF functions. However, this vascular regression may lead to hypoxia in tumors and upregulation of VEGF production, which stimulates tumor revascularization after either prolonged exposure to the drugs or during interruptions in treatment. Essentially, a blockade of angiogenic signaling therapy suppresses the growth of newly formed tumor vessels, but is less effective against the more established tumor vasculature.

An alternative approach to anti-angiogenic signaling therapy is to target VEGFR for selective delivery of highly cytotoxic agents into endothelial cells; with the expectation that only tumor endothelial cells overexpressing such receptors will internalize therapeutically significant amounts of VEGFR-targeted cytotoxins. Since alternative signal transduction pathways cannot prevent or reverse the cytotoxic activity of plant or bacterial toxins, several groups have investigated recombinant proteins fused to VEGF for targeting such toxins to tumor vasculature.[8,9] One such recombinant protein, known as SLT-VEGF, is comprised of a human VEGF121 protein fused to the A subunit of the Shiga-like toxin (SLT), a site-specific N-glycosidase that when internalized, cleaves off adenosine at position 4324 in 28S rRNA. This modification prevents the ribosome from properly interacting with elongation factors thus blocking protein synthesis and eventually leading to cell death. SLT-VEGF is highly cytotoxic to VEGFR-2 overexpressing cells *in vitro*, and selectively reduces such cells in tumor vasculature.[8] The aim of this study is to test SLT-VEGF for its ability to sustain inhibition of tumor angiogenesis when used in combination with an angiogenesis signaling pathway inhibitor such as the small molecular drug Sutent (Sunitinib).

Problem:

As conventional therapies for treating CNS tumors have been shown to be ineffective, an approach to target tumors by depriving them of their blood supply should be evaluated as a method that avoids both intrinsic and acquired resistance.

Goal:

The goal was to...

1. Follow the dynamics of vascular remodeling after 5-day Sutent treatment and then determine if there is a correlation between the activity of VEGFR-2 promoter (as shown by luciferase activity) and vascular remodeling as shown by in vivo cell tagging and fluorescent microscopy;
2. Test SLT-VEGF for its ability to sustain inhibition of tumor angiogenesis when used in combination with an angiogenesis signaling pathway inhibitor, such as the small molecule drug Sutent.

Hypothesis:

It was hypothesized that...

1. There will be a correlation between VEGFR-2 promoter activity and vascular remodeling because VEGF is considered to be a key regulatory molecule in angiogenesis that induces vascular growth and permeability and acts as a survival factor for newly formed vessels;
2. SLT-VEGF will selectively target and inhibit protein synthesis of cells with high VEGFR-2 expression.

Results & Discussion

BLI and NIRF imaging was performed on mice anesthetized with a ketamine/ xylazine mixture (30 ul/mouse i.m). This amount was sufficient to anesthetize mice for one hour. After mice were anesthetized they receive i.p. injections of 100 ul of scVEGF/Cy (50 uM) followed 10-15 minutes later with 0.6 ml aqueous luciferin (3 mg/ml).

FaDu and U87 tumors grew despite Sutent or SLT-VEGF treatment. BLI showed half as much intensity in tumors of Sutent-treated mice as untreated control mice while BLI tumors of SLT-VEGF treated mice were as strong as in the control mice. NIRF was barely detectable in either control or Sutent-treated mice. After imaging mice were sacrificed and their tumors excised for immunohistochemical analysis of the tissue. The statistics we did on the image analysis was a one-way analysis of variance (ANOVA) on the ratios of pixel intensity of CD31 staining over DAPI (diamidino-2-

phenylindole; used for blue-florescent DNA) staining. Staining ratios of the three groups were compared for statistical significance by the Bonferroni multiple comparison procedure. After treatment was administered (SLT in combination with Sutent, and just Sutent), data was shown as seen in Figures 3, 4 and 5. As shown in the figures, the recovery group was statistically higher than the control group throughout both FaDu and U87 groups.

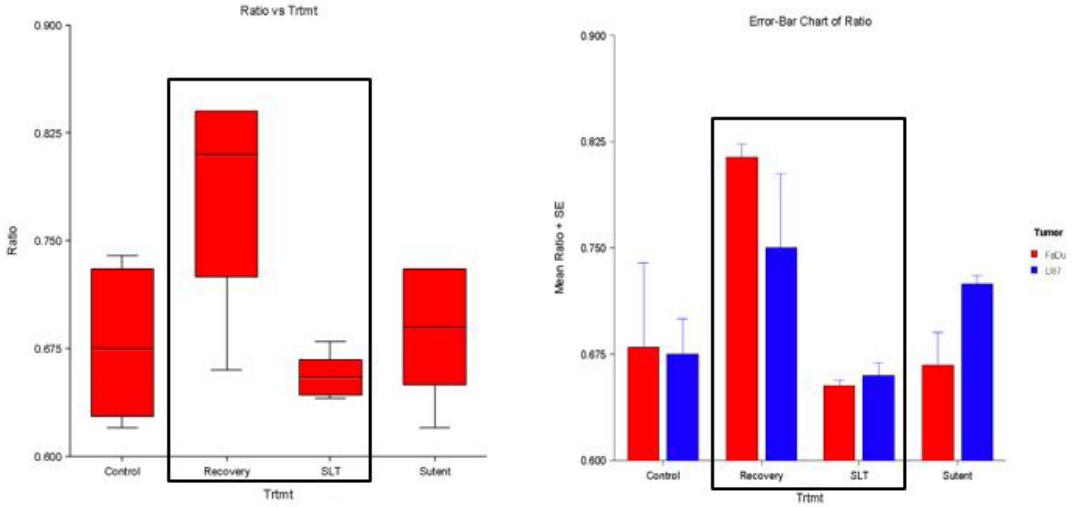

Figure 3: As shown, the recovery group is statistically higher than the control group, proving that the lowest ration in SLT group is significant.

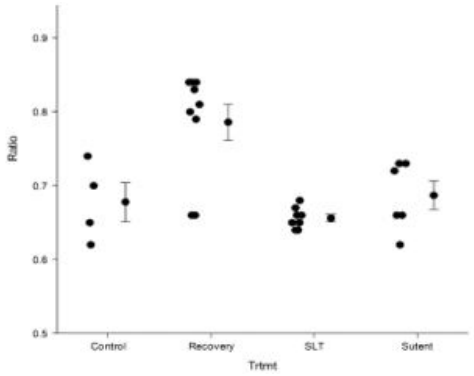

Figure 4: SLT-VEGF treatment significantly inhibits rebound of CD31 expression after recovery from Sutent treatment. Pixel ratios measured with ImageJ software.

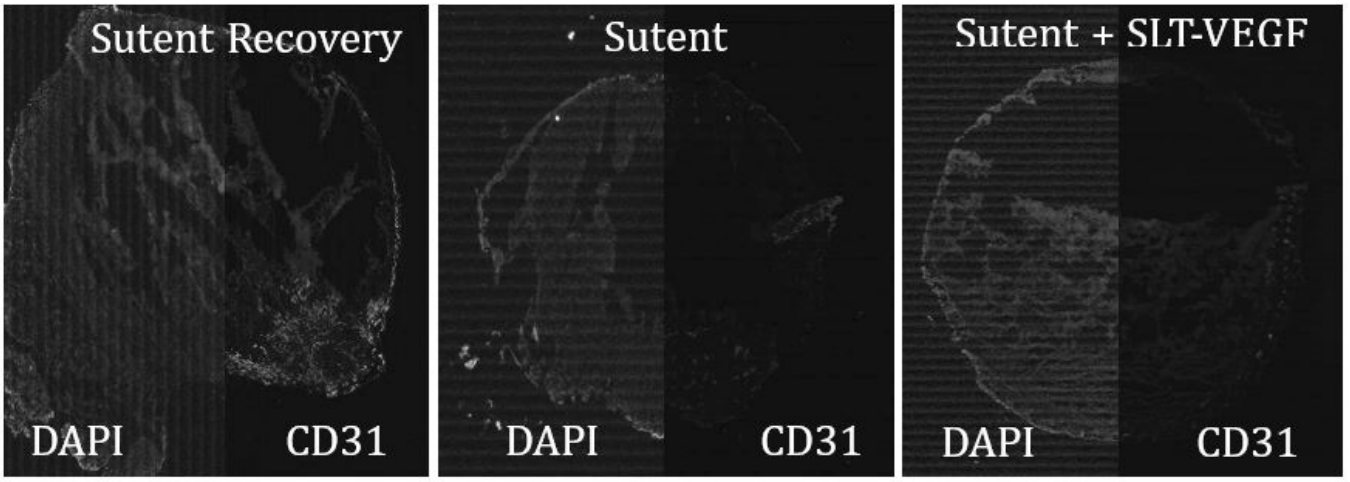

Figure 5: As shown in these data examples, the recovery group is statistically higher than the control group, proving that the lowest ration in SLT group is significant. DAPI staining represents all tumor cells, whereas CD31 represents vasculature.

Anti-angiogenic therapy represents a promising alternative to the treatment of malignant brain tumors that avoid the problems of conventional therapies. It seems likely that a combination of anti-angiogenic agents, with other cytotoxic therapies, will be required to achieve maximal efficacy. In this study the combination of SLT-VEGF, a fusion toxin that

enters the cell via VEGF receptor mediated endocytosis, and depletes VEGFR-2+/CD31+ endothelial cells from the vasculature, and Sutent, a receptor protein-tyrosine kinase inhibitor, was evaluated for inhibiting tumor angiogenesis in two models of human and rat brain tumors. The treatment inhibits the actions of vascular endothelial growth factor (VEGF) and is an angiogenesis inhibitor. In this experiment, four main groups of treatments were created, and given to nude mice (medulloblastoma tumors). In the group with no treatment, the tumor had maximum amounts of blood vessel networks (figure 4). The Sutent treatment has slightly fewer networks however, as expected, after Sutent treated issues were allowed to "recover," the vessel networks were re-established. One of the main reasons this may have occurred (other than the previously predicted signaling pathway resistance) could have been through the formation of pericytes. Pericytes, or contractile cells that wrap around the endothelial cells that line capillaries and venules throughout the body, were formed on the edge of these CNS Sutent treated tumors. Thus, an acquired resistance was formed, and a need for a drug with two preventative behaviors is necessary. Thus, when SLT was administered, and given a time period for recovery, the pixel count was significantly less. Administering SLT-VEGF with Sutent effectively prevented the rebound effect.

Conclusions

The key issues here are that glioblastoma, medulloblastoma, and other CNS tumors (the most malignant forms of infiltrating astrocytoma's) can evolve from lower-grade precursor tumors to higher grade lesions. Underlying genetic alterations in these CNS tumors may tilt the balance in favor of an angiogenic phenotype by upregulation of proangiogenic factors and downregulation of angiogenesis inhibitors. Increased vascularity and endothelial cell proliferation are also driven by hypoxia-induced expression of proangiogenic cytokines, such as VEGF. Selective targeting of VEGFR (overexpressed receptor of VEGF) in tumor vasculature with VEGF conjugated with a radioactive isotope 177/Lu has been shown to be effective in orthotopic breast cancer models. As high levels of VEGFR expression in tumor vasculature are a common feature in a variety of cancers, included glioblastoma and other brain tumors, we found that non-radioactive VEGFR-targeting compounds was an effective anti-tumor therapy in anti-angiogenic therapy.

Methods

Animals and cell lines

Transgenic VEGFR2/Luc mice were obtained from Caliper and maintained in the Comparative Medicine Department of New York Medical College under an approved IUCAC protocol. The rat glioblastoma cell line FaDu (Catalog number HTB-437) and human Uppsala 87 Malignant Glioma (U87) were obtained from the American Type Culture Collection (ATCC) and maintained in culture with RPMI-1640 medium supplemented with 10% fetal calf serum and 2 mM L-glutamine.

Sunitinib for Oral administration

90 ml of sterile DI was warmed in a glass beaker to ~80°C on a magnetic stirrer/ hot plate. 0.5 g of CMC was added and stirred vigorously for five minutes. The heat was turned off, and CMC stirred slowly for 16-18 hours until dissolved, at that point 1.9 g of NaCl, 4 ml 10% Tween 80, and 0.9 ml of benzyl alcohol were added and stirred until complete homogeneity was achieved. The volume was adjusted to 100ml with sterile DI and the resulting CMC stock solution was distributed in 10 ml aliquots in 15-ml conical tubes and stored at RT.

100 mg of Sutent was weighed and distributed into six 1.5-ml tubes containing approximately 1 ml of CMC. The Sutent mixture was vortexed at high speed for five min then all tubes were placed in a water bath sonicator, and sonicated on a high setting for 10 min. When all tubes became uniformly an orange-yellow color, the suspensions were collected in the original 15ml conical tube with the leftover CMC. The final concentration of the Sutent was 10 mg/ml. After sterilization by autoclaving the Sutent suspension was stable for 1-2 weeks in a refrigerator under constant agitation. The final concentration of ingredients included 0.5% CMC, 1.8% NaCl, 0.4% Tween 80 (Acros Organics, Cat #278632500, Belgium), and 0.9% Benzyl alcohol (Fluka, Cat #77013, Canada).

Reagents and Kits

Rat Anti-mouse Flk1 and PECAM/CD31 antibodies (BD Bioscience), rat IgG (Zymed), normal rabbit serum and biotinylated rabbit anti-rat IgG (Vector Labs), a biotin blocking kit and TSA-488 HRP-streptavidin kit (Molecular Probes) were all refrigerated at -20°C). 16% Formaldehyde (Polysciences) was stored at RT and Vector Shield Mounting medium (Vector Labs) was refrigerated. Tyramide stock was used to dissolve component A in 150 µL of DMSO (component B) and stored in small aliquots at 20°C. The HRP-streptavidin conjugate was reconstituted

in 200 µL PBS which was stable for up to 9 months at 4°C. The 10x blocking reagent was made in PBS, and 1-ml aliquots were stored at 20°C. The 10x concentrate was diluted with 1xPBS immediately before staining. The 10xPBS, concentrate was obtained from USB Corporation (75889), and the antibody diluent was obtained from BB Bioscience (55914).

Sunitinib treatment of tumor bearing mice

Mice bearing FaDu and U87 tumors were dosed with Sunitinib via gastric gavage. Sunitinib malate salt (Sutent, LC Laboratories, S-8803 Lot BST-102, City, State) was prepared as a suspension with carboxymethylcellulose (CMC, Fluka, Cat #21904, City, State) as described above.

Bioluminescent Imaging (BLI) and Near Infrared Fluorescence (NIRF) of tumor bearing mice

BLI and NIRF were used to detect endogenous luciferase in transgenic mice under control of a VEGFR-2 promoter. Tumors were established by inoculating $2x10^6$ U87 cells subcutaneously in the right flank and 2 $x10^6$ Fadu cells subcutaneously in the left flank of mice. After tumors had reached a diameter of approximately 0.5 cm in diameter, mice were anesthetized with an intramuscular (i.m.) injection of 40 ul of a mixture of Ketamine (100 mg/ml, Fort Dodge Animal Health, Fort Dodge, KS) and Xylazine (100 mg/ml, Akron Incorporation, Akron, OH). Mouse eyes were covered with an ocular lubricant (Pharmaderm) during the procedure. BLI and NIRF images were acquired with a LAS 4000 Imager (Fujifilm, City, State). Prior to imaging mice were anesthetized as described above and injected i.p. with 1 ml of aqueous luciferin (5 mg/ml, Molecular Imaging Cat. # LUC 00, City, State). For NIRF a solution of ScV/AI 594 (Sibtech, Lot #3) reconstituted in PBS to 50 uM and scVEGF/Cy (Sibtech, Lot #27) were injected in a 0.1 ml volume per mouse via the retro-orbital plexus. After imaging experiments were completed, mice were sacrificed and tumors were removed and frozen in O.C.T Compound (Tissue-Tek) for immunohistological studies.

Fluorescent Staining of Tissue Cyrosections

The frozen slides of tumor tissue cut with a cryostat were removed from the freezer and allowed to come to room temperature (10-30 min). A circle was drawn around the tissue section with a PAP pen and let dry for 1-2 min. Slides were labeled with permanent, solvent-resistant Marker/Superfrost. A 1% blocking solution in PBS (1 ml 10% protein concentrate stored at -20°c + 9 ml PBS) and a 1% formaldehyde solution (one 10ml vial of 16% formaldehyde + 150ml PBS) were freshly prepared. The working rat IgG (specificity control) was made by diluting rat IgG (2.5mg/ml) 1:25 with antibody diluent to give a final 0.1 mg/ml concentration. It was kept at +4°C. Slides were fixed in 1% formaldehyde 10 min at RT. Excess liquid was drained off and it was washed in PBS, 2x5 min. A stock 30% H_2O_2 solution was diluted 1:100 to a final concentration of 0.3% in a coplin jar (0.5 ml + 50 ml PBS). Slides were put in the jar for 10 min, after which, H_2O_2 was dumped off and slides were washed in PBS, 2x5 min. Slides were quenched once more with 30% H_2O_2 stock diluted to 1% (1.5ml H_2O_2 + 45 ml PBS).

ImageJ Analysis

ImageJ program was used (which is freely available from NIH) to determine the percentage of pixels that were positive for staining of CD31 and DAPI separately in a defined region of interest (ROI) for each image. DAPI staining represented the number cells within a ROI and the ratio of CD31 percent staining/DAPI percent staining was calculated to estimate the total percent of cells stained with CD31 in each image. These ratios were then compared by one-way ANOVA (to determine whether there are any statistically significant differences between the means of two or more independent (unrelated) groups) in CD31 expression between each treatment group.

Acknowledgements

This project was made possible by mentor Carl V. Hamby (from the New York Medical College), and teachers Michael Blueglass and Rachel Koenigstein.

References

1. “Brain Tumor Statistics.” Brain Tumor Statistics | American Brain Tumor Association, www.abta.org/about-us/news/brain-tumor-statistics/.
2. “National Center for Biotechnology Information.” National Center for Biotechnology Information, U.S. National Library of Medicine, www.ncbi.nlm.nih.gov/.
3. Lakka, Sajani S, and Jasti S Rao. Antiangiogenic Therapy in Brain Tumors. Oct. 2008, www.ncbi.nlm.nih.gov/pmc/articles/PMC2656359/?report=reader.
4. Jain, Rakesh K, et al. Angiogenesis in Brain Tumours. Aug. 2007, www.bing.com/cr?IG=5B991BCBC1684E558CDEAF6E00E8611C&CID=1121BE06595E6F2F32BDB59A58F16E4D&rd=1&h=4nGCkR7uAkoADkSYHs78LdFydVRK-71eku0qO8njpeI&v=1&r=http%3a%2f%2fwww.nature.com%2fnrn%2fjournal%2fv8%2fn8%2fabs%2fnrn2175.html&p=DevEx,5072.1.
5. “Angiogenesis Inhibitors.” National Cancer Institute, www.cancer.gov/about-cancer/treatment/types/immunotherapy/angiogenesis-inhibitors-fact-sheet.
6. Vasudev, Naveen S., and Andrew R. Reynolds. Angiogenesis, Springer Netherlands, 2014, www.ncbi.nlm.nih.gov/pmc/articles/PMC4061466/.
7. Ackerman, Rachel, et al. “SLT-VEGF Reduces Lung Metastases, Decreases Tumor Recurrence, and Improves Survival in an Orthotopic Melanoma Model.” MDPI, Molecular Diversity Preservation International, 27 Aug. 2010, www.mdpi.com/2072-6651/2/9/2242.
8. Hotz, Birgit, et al. Neoplasia (New York, N.Y.), Neoplasia Press Inc., Oct. 2010, www.ncbi.nlm.nih.gov/pmc/articles/PMC2950329/.

Author

Shrila is grateful to have conducted a project that closely regards her passion in entering the medical field and majoring in biology. Shrila has always been interested in research and hopes to continue studying brain tumors along with learning about other types of cancer.

The International Journal of High School Research is published by
Terra Science and Education